

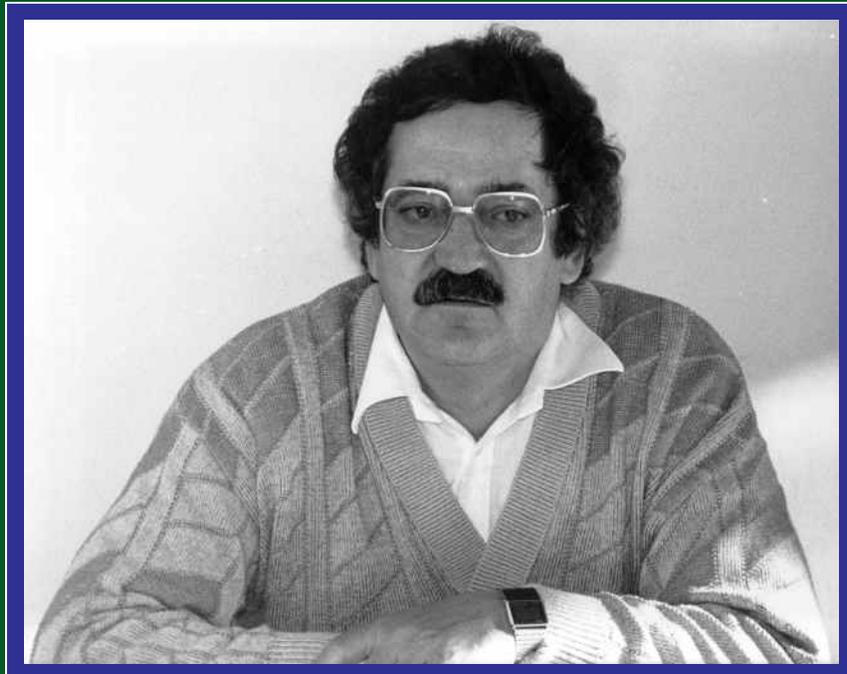
AJP

ISSN : 0971 - 3093

Vol 25, No 2, February, 2016

ASIAN JOURNAL OF PHYSICS

An International Quarterly Research Journal



ANITA PUBLICATIONS

FF-43, 1st Floor, Mangal Bazar, Laxmi Nagar, Delhi-110 092, India
B O : 2, Pasha Court, Williamsville, New York-14221-1776, USA



The accuracy of the M06L DFT method in the prediction of the vibrational Spectra of 4-amino-2-chlorobenzonitrile: A detailed interpretation of the Molecular Structure and vibrational IR and Raman spectra and other molecular properties using several DFT methods

M Alcolea Palafox^a, Anupama^b, Rachna Rastogi^{c*}, M Jane Alam^d, Daisy Bhat^e, and V K Rastogi^{c,e}

^a*Nofima AS - the Norwegian Institute of Food, Fisheries and Aquaculture Research, PB 210, N-1431 Ås, Norway.*

^b*Department of Chemistry, SRM University, NCR Campus, Modinagar-201 204, India.*

^c*Indian Spectroscopy Society, KC 68/1, Old Kavinagar, Ghaziabad-201 002, India.*

^d*Department of Physics, Aligarh Muslim University, Aligarh, India.*

^e*Internet Lab, R D Foundation Group of Institutions, NH-58, Kadarabad (Modinagar), Ghaziabad, India.*

Dedicated to Professor Wolfgang Kiefer on the occasion of his 75th birthday

The accuracy of the M06L DFT method in the prediction of the vibrational spectra of 4-amino-2-chlorobenzonitrile molecule was tested and compared with that of the B3LYP method. The experimental FT-IR and FT-Raman spectra in the solid state were recorded at room temperature, and the bands assigned with accuracy by comparison with the results obtained by different methods, including MP2 and DFT. The FT-IR spectrum in Nujol mull was also recorded and analyzed. Several scaling procedures were used and several recommendations were presented. The wavenumbers of most of the modes were found in the expected range and the error obtained was in general very low. The thermodynamic parameters were calculated and discussed. The NBO analysis was done and Molecular Electrostatic Potential (MEP) was plotted. The calculated HOMO and LUMO energies showed that charge transfer occurs within the molecule. Several general conclusions were deduced. © Anita Publications. All rights reserved.

Keywords: M06L DFT method; FT-IR and FT-Raman spectra; Molecular Electrostatic Potential (MEP); HOMO and LUMO.

1 Introduction

The theoretical prediction of vibrational spectra is of practical importance and has become an important part of spectrochemical and quantum chemical investigations. A variety of different approaches combining the theoretical and experimental results for predicting accurate vibrational wavenumbers have been suggested and reviewed by us [1-3]. However, the accuracy of one of the new DFT methods, the M06L, has not been tested yet from the spectroscopic point of view. Thus, the main aim of the present manuscript was to present scaling equations to be used with this method and to determine the accuracy obtained with them in a simple BN derivative, the 4-amino-2-chlorobenzonitrile molecule (4A-2CBN), which has not been analyzed yet completely. Thus all the results obtained in the present study are being reported for the first time.

4A-2CBN molecule was selected for the present study because of the interesting biochemical and physical properties of benzonitrile (in short BN) and its amino derivatives. Substituted benzonitriles have been studied extensively due to their wide applications in various fields, e.g. they are used in the

Corresponding author :

e-mail: alcolea@ucm.es (M Alcolea Palafox); v_krastogi@rediffmail.com (V K Rastogi)

manufacturing of polymers and anhydrous metallic salts and as well as intermediates for pharmaceuticals, agrochemicals, pesticides and other organic chemicals [4-8], and also they have many other important applications [9-12]. Several halogen derivatives are well known herbicides since 1960s, and it was found that benzonitriles, substituted at the 2 and 6 positions by halogen or methyl, had the highest herbicidal activity. 2,6-dichlorobenzonitrile (2,6-DCBN) is a contact herbicide which controls broadleaf weeds in grass type crops and in cranberry bogs. Some 2,6-dichloro-1-substituted benzene derivatives showed herbicidal activity, comparable with that of 2,6-dichlorobenzonitrile. 2,6-difluorobenzamide, a fluorinated derivative of DCBN, is used to synthesize benzyl urea like pesticides. Due to the high electro-negativity of chlorine atom, entirely different physical and chemical properties are observed in these compounds as compared to the other halogenated derivatives [13-16].

Although numerous experimental studies using the IR and Raman spectroscopic techniques, and theoretical ones have been made in recent years on the vibrational spectra of BN and its mono- and di-substituted derivatives [17-36], however, as far as we know, no structural data and a complete rigorously studied vibrational analysis on 4A-2CBN molecule, Fig 1, are available in literature yet [37]. Therefore, the another aim of the present work is to analyze in detail for the first time the molecular geometry and vibrational spectra of this molecule. The assignments and interpretation of the experimental IR and Raman bands are based on DFT calculations and accurate scaling. Also, the results of the NLO properties, MEP mapping and HOMO-LUMO analysis for the title compound are discussed for the first time. The importance of this molecule may be seen from the fact that the substituted benzonitriles are finding increasing applications in a variety of fields.

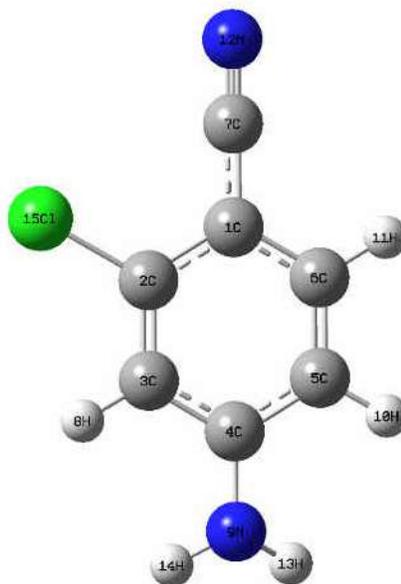


Fig 1. Label of the atoms in 4A-2CBN molecule.

2 Experimental

The compound 4A-2CBN ($C_7H_5ClN_2$) of spectral grade in solid state was purchased from M/s Aldrich Chemicals (Milwanke, WI USA) and used as such without any further purification. The FTIR spectrum of this compound in KBr pellet (with 1 mg sample per 300 mg KBr) was measured on a Perkin Elmer FT-IR Model 1760 X, while the infrared spectrum in nujol mull was recorded on Nicolet DX spectrometer. The spectra are shown in Figs 2-3.

The FT-Raman spectrum was measured on a Nicolet Raman 950 instrument operating at room temperature. The spectrum was recorded in powder form in the region of $3500\text{-}0\text{ cm}^{-1}$. The spectrum was accumulated by acquisition of 400 scans at a fixed temperature. The sample was mounted in the sample illuminator using an optical mount and no sample pretreatment was undertaken. The NIR output (1064 nm) of an Nd:YAG laser was used to excite probe. The instrument was equipped with InGaAs detector. The instrument was set at 250 mW. The spectra are shown in Figs 4-5.

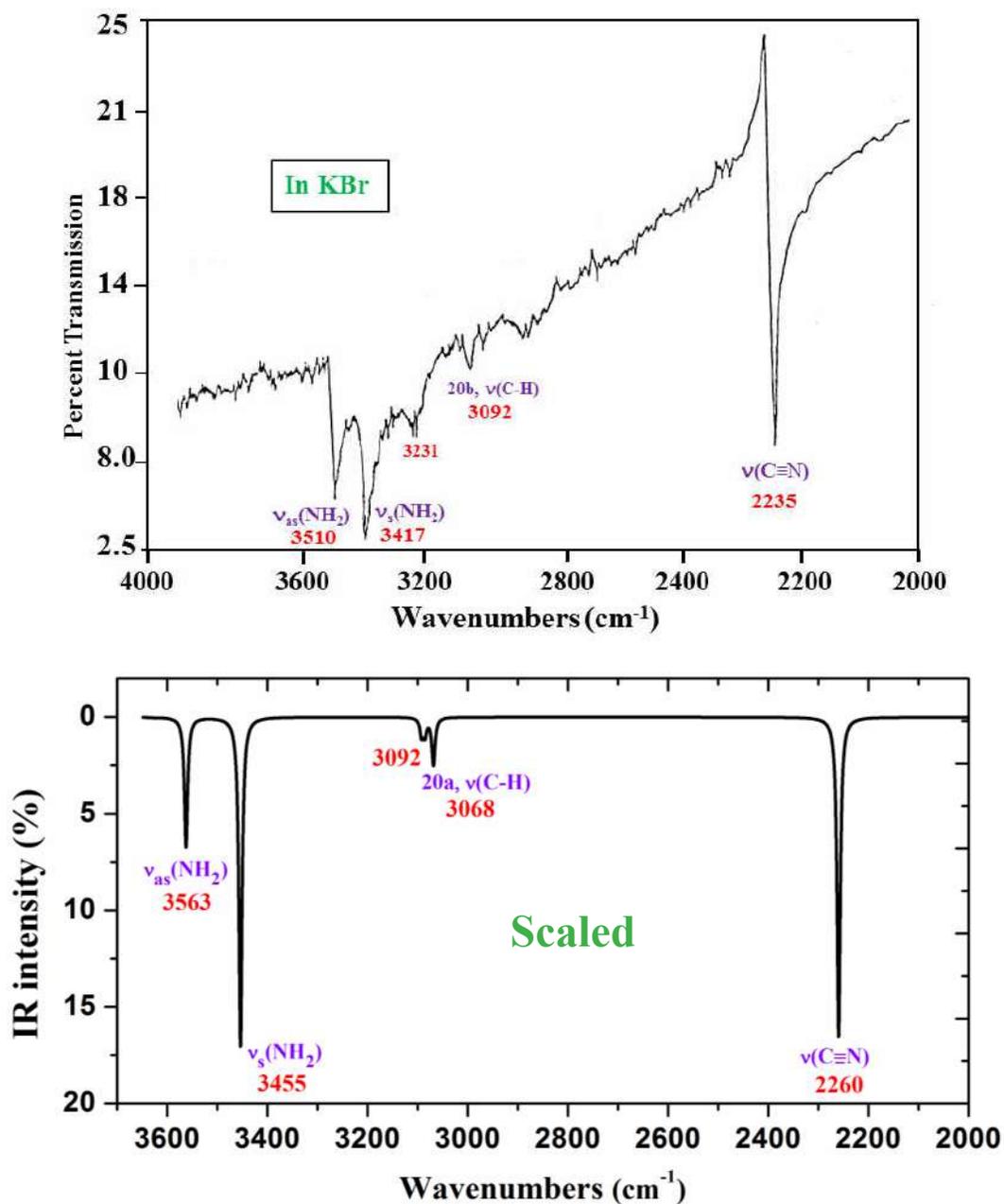


Fig 2. Calculated (scaled) and experimental IR spectra in KBr matrix of 4A-2CBN in the $4000\text{-}2000\text{ cm}^{-1}$ range.

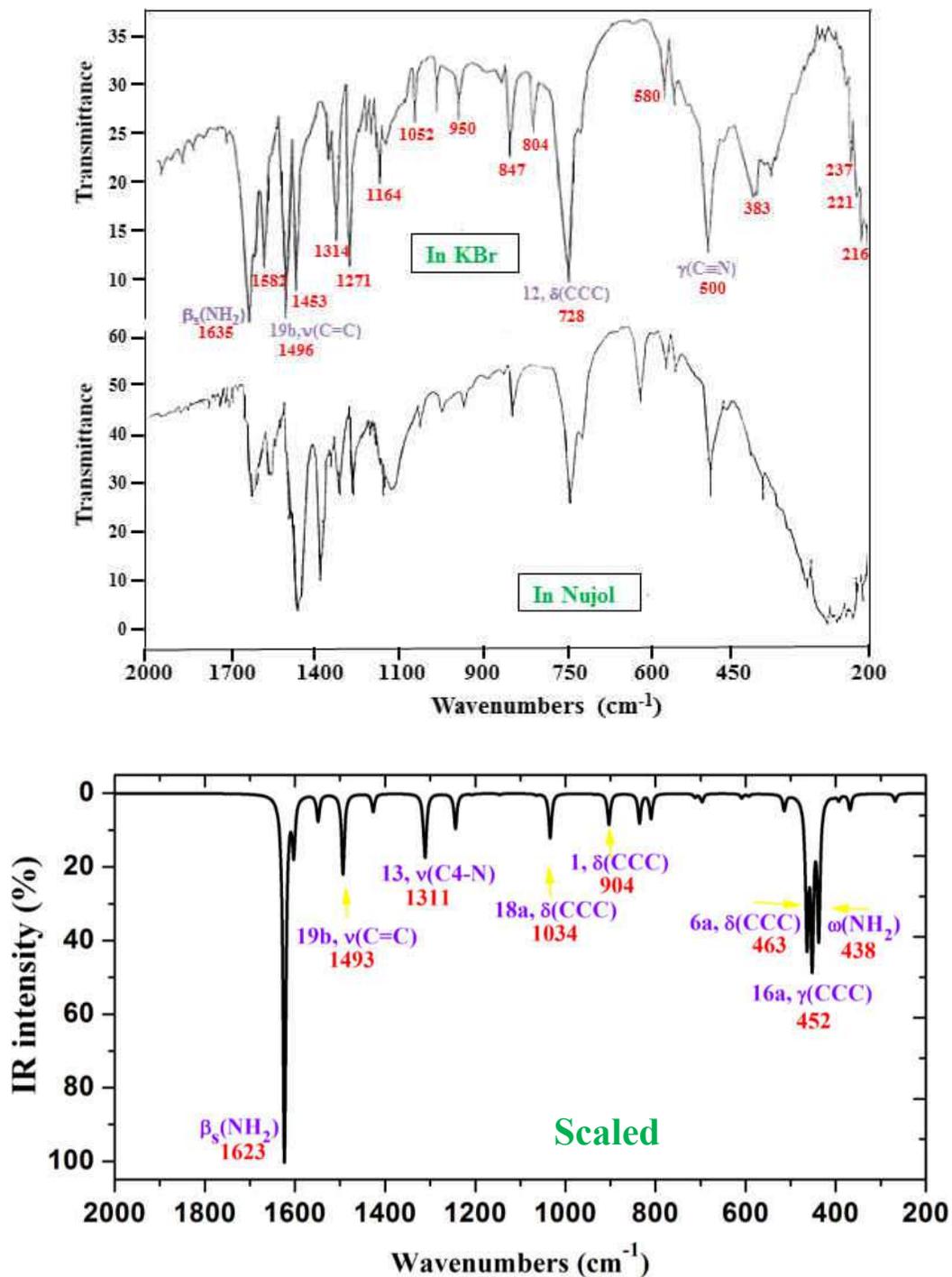


Fig 3. Experimental IR spectra of 4A-2CBN molecule in the 2000-200 cm^{-1} range in KBr and Nujol matrix, and theoretical scaled spectrum using the scale equation procedure.

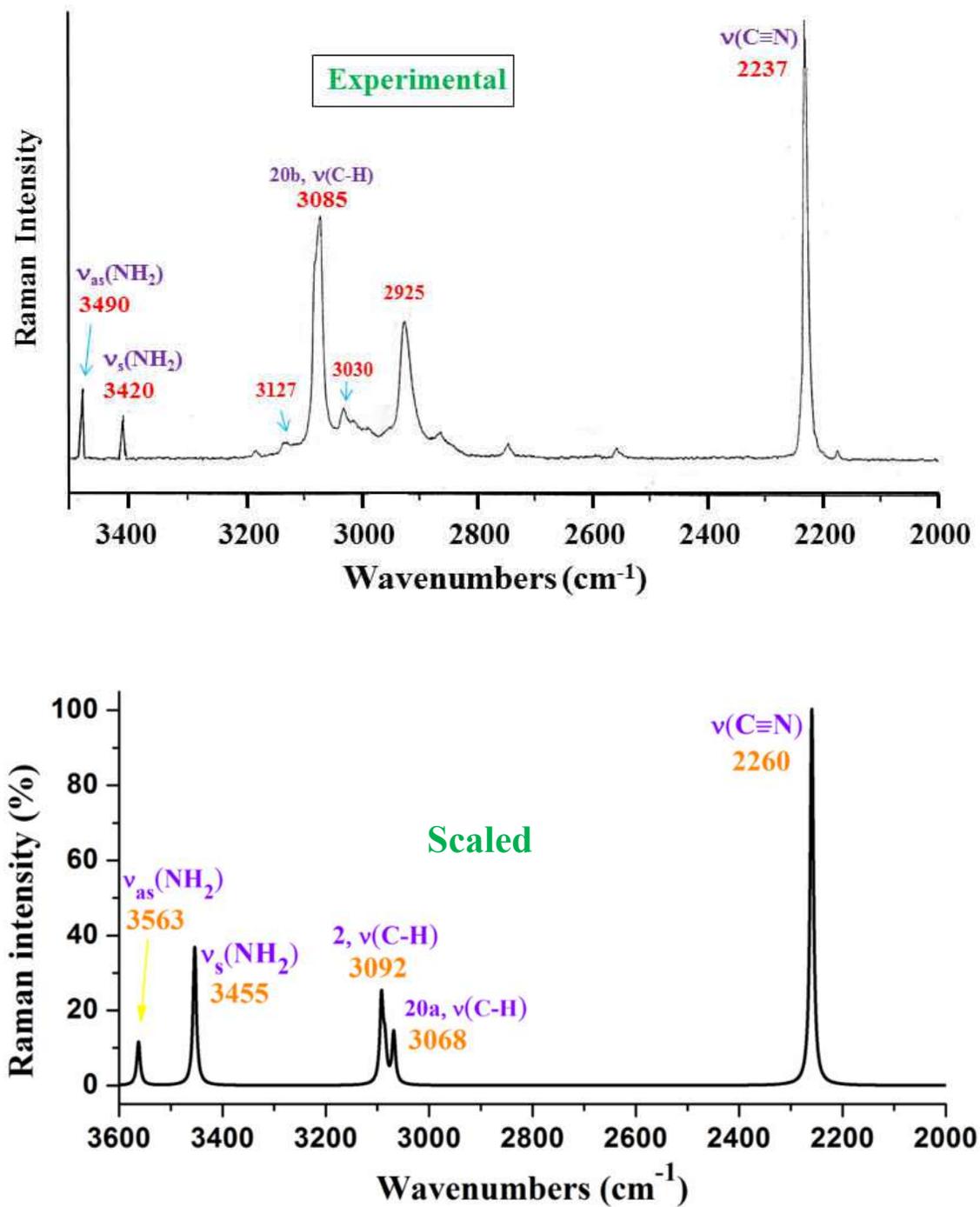


Fig 4. Experimental and theoretical scaled Raman spectrum in the 3500-2000 cm⁻¹ range using the scale equation procedure with benzene molecule.

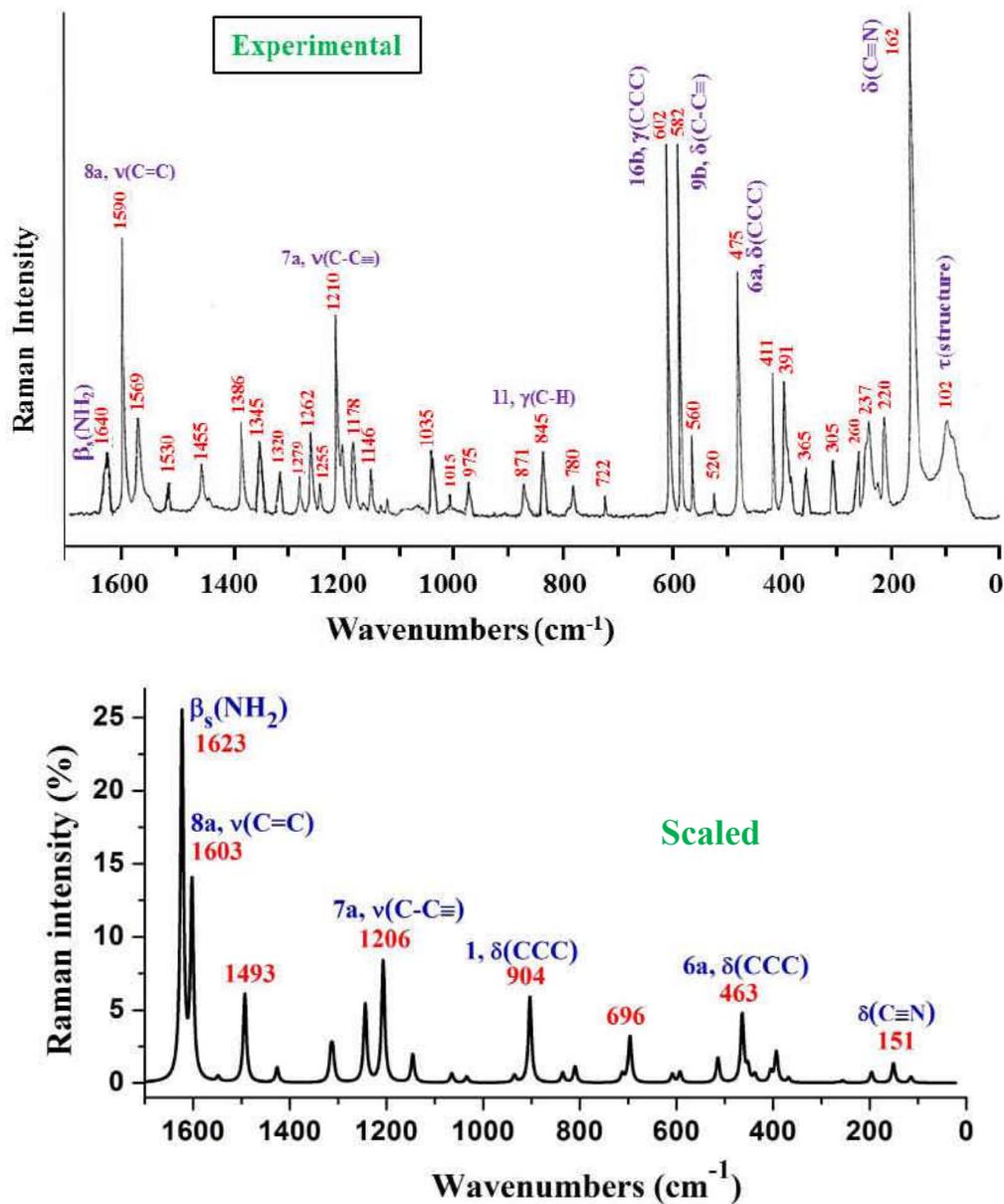


Fig 5. Experimental and theoretical scaled Raman spectrum in the 1700-0 cm⁻¹ range using the scale equation procedure with benzene molecule.

3 Computational details

Ab initio HF (Hartree-Fock), MP2 (second-order Møller-Plesset) and DFT methods are most commonly used for the calculations of vibrational normal modes of a molecule to interpret and understand its experimental vibrational (infrared and Raman) spectra. In the calculations done by these methods, the effect of anharmonicity on both the vibrational frequencies and on the IR and Raman intensities is neglected. Therefore, the calculated harmonic frequencies and IR and Raman intensities, in many cases, are not in good

agreement with the experimentally observed IR and Raman spectra [38]. In the present study, the density functional theoretical (DFT) computations [39] were performed because they provide a very good overall description of medium-size molecules. Moreover, for the wavenumber calculations [1-3,40] they appear more accurate than HF and MP2, and at lower computational cost.

Mainly, three levels of theory have been used for geometry optimisation and calculations of vibrational wavenumbers: B3LYP/6-31G(d,p), B3LYP/6-311++G(3df,pd), and M06-L/6-31G(d,p). Among the DFT methods, B3LYP is the most popular, and it has been used satisfactorily in many studies of DNA components [41-46], of drug designing [47-49], and of several other important molecules [50-54]. With these methods and basis sets we have recently studied the geometry, and molecular properties of a series of dichlorobenzonitriles and difluorobenzonitriles [32,33, 54-57].

In the present study, the results obtained by B3LYP method were compared with those obtained with the new local density functional method M06L [58] available today in Gaussian 09 [59] program package, and developed by Zhao and Truhlar [60]. M06L generally yields good results for a broad range of interactions, including non-covalent interactions [58,60]. However, the accuracy of M06L in the calculation of the vibrational wavenumbers has not been tested yet, although several studies with M06 method have been reported [61].

The geometry structure and atomic charges calculated by DFT methods were confirmed by using *ab initio* MP2 calculations. For comparison purposes the natural NBO atomic charges [62,63] were also calculated in BN molecule.

Molecular geometries were fully optimized by Berny's optimization algorithm in redundant internal co-ordinates, and with the standard optimization convergence criteria. Imaginary frequencies were not found in the vibrational analysis which proves that the geometries determined belong to a true minimum. The harmonic approximation was used at the same level of theory that the optimized geometry. Visualization and checking of calculated data were done by using the Gauss View 4.1 program for the stable form of the molecule.

Raman scattering activities (S_i) calculated by Gaussian 09 program were suitably converted to relative Raman intensities (I_i) using the following relationship derived from the basic theory of Raman scattering [64-66]:

$$I_i = \frac{f(\nu_0 - \nu_i)^4 S_i}{\nu_i [1 - \exp(-h\nu_i / kT)]}$$

where f is the suitable chosen common scaling factor for all the peak intensities, ν_0 is the laser exciting frequency (cm^{-1}); in this work we have used the exciting wavenumber $\nu_0 = 9938.5$ (which corresponds to the wavelength of 1064 nm of a Nd:YAG laser), ν_i is the vibrational wavenumber of the i th normal mode, and h , c and k are universal constants.

4 Results and Discussion

4.1 Geometry Optimization

The optimized bond lengths, bond angles and torsional angles determined by the different theoretical methods in the isolated state of 4A-2CBN molecule are listed in the 2nd to 5th columns of Table 1, while the labeling of the atoms is plotted in Fig 1. Although X-ray experimental data on 4A-2CBN has not been reported yet, however, the calculated values with the different methods were, in general, in accordance to the microwave data reported for the molecule of BN [67], to the X-ray values in 4-aminobenzonitrile (4ABN) [55b-d], and to the computed values in several BN derivatives [25,26]. In the crystal of the solid state, the molecules of 4A-2CBN are expected to be connected to a three-dimensional network, as reported in 4ABN [68-70], and to form intermolecular H-bonds between an amino H-atom and the cyano group of a

neighboring molecule, with classical hydrogen bonds of the N–H···N type. As a consequence, an unexpected small deviation from co-planarity for the phenyl and cyano groups can be predicted. Also, in the crystal the cyano group is expected to appear bent towards the substituent amino group.

Table 1. Optimized geometrical parameters at B3LYP, M06L and MP2 levels in 4A-2CBN and benzonitrile (BN) molecules.

Parameters	4A-2CBN				BN	
	B3LYP/ 6-31G(d,p)	B3LYP/ 6-311++G(3df,pd)	M06L/ 6-31G(d,p)	MP2/ 6-31G(d,p)	B3LYP/ 6-31G(d,p)	MP2/ 6-31G(d,p)
<i>Bond lengths</i>						
C1-C2	1.408	1.403	1.407	1.404	1.405	1.403
C2-C3	1.387	1.382	1.384	1.39	1.392	1.393
C3-C4	1.408	1.401	1.404	1.402	1.397	1.397
C4-C5	1.41	1.404	1.407	1.405	1.397	1.397
C5-C6	1.383	1.378	1.38	1.387	1.392	1.393
C6-C1	1.409	1.402	1.406	1.404	1.405	1.403
C1-C7	1.428	1.423	1.42	1.43	1.435	1.436
C2-Cl	1.749	1.734	1.734	1.734	-	-
C4-N	1.38	1.377	1.374	1.392	-	-
C≡N	1.164	1.153	1.169	1.184	1.163	1.184
<i>Bond angles</i>						
C2-C1-C6	117.6	117.8	117.5	118.5	120.1	120.5
C-C2-C	121.5	121.2	121.5	120.8	119.7	119.4
C-C3-C	120.3	120.5	120.2	120.5	120.2	120.3
C-C4-C	118.7	118.7	118.8	118.9	120.2	120.1
C-C5-C	120.3	120.3	120.3	120.4	120.2	120.3
C-C6-C	121.5	121.5	121.6	120.9	119.7	119.4
C2-C1-C7	122.5	122.3	122.1	121.7	120	119.7
C6-C1-C7	119.9	119.9	120.4	119.8	120	119.7
C1-C2-Cl	120	120.1	119.7	120.3	-	-
C3-C2-Cl	118.5	118.7	118.8	119	-	-
C3-C4-N	120.4	120.4	120.3	120.3	-	-
C5-C4-N	120.8	120.8	120.8	120.6	-	-
C-C≡N	179.9	178.1	178.3	178.3	180	180
H-N-H	114	114.2	113.8	111.4		
ε tilt angle	2	2.1	1.4	4.6		
ω (inversion)	32.5	31.5	33.3	42.1		
<i>Torsional angles</i>						
C2-C-C4-N	177.6	177.7	177.4	177		
C3-C-N-H14	20.3	19.6	20.6	26.9		
C5-C-N-H13	-20.5	-19.7	-21.3	-27.6		

Two optimum conformations were determined in 4A-2CBN molecule, with the planar form of the -NH₂ group being saddle point. Thus, the data on this conformer were omitted in the present manuscript. With the exception of this -NH₂ group, in the stable form the molecule is completely planar. The nitrogen atom is ca. 0.10 Å above the plane of the phenyl ring (at MP2 level) with both hydrogen atoms in opposite directions.

Phenyl-ring structure

As compared to MP2 values, the calculated C-C bond lengths by B3LYP appear with the same accuracy as that by M06L. However, the C-C1 bond length computed by M06L has the same value as that by MP2, while by B3LYP/6-31G(d,p) it is 0.015 Å longer. The calculated C≡N bond length by B3LYP and M06L are noticeably lower than by MP2, i.e. these methods (B3LYP and M06L) appear to fail in the calculation of C≡N bond length, although the difference is larger by B3LYP than by M06L.

For comparison purposes the values obtained in BN molecule were also collected in the 6th-7th columns of Table 1. The broad features observed by the replacement of the hydrogens in positions 2 and 4 of the BN moiety by chlorine and amino substituents, respectively, can be described as follows:

(i) The effect of the chlorine atom on the ring bond lengths is small; at the MP2 level the C1-C2 and C1-C6 bonds have the same value, while C2-C3 is only 0.003 Å longer than C5-C6. The effect on the angles is also very small or almost null, with very close value for C1-C2-C3 and C1-C6-C5.

(ii) The increment of the lengths in the C-C bonds adjacent to C1-C7 and C4-N10 is accompanied by slightly irregular hexagonal structure, measured in the *ipso* angles C2-C1-C6 and C3-C4-C5, with values at the MP2/6-31G(d,p) level of 118.5° and 118.9°, respectively. These values are in agreement with that calculated at the same level by us in the aniline molecule [71], 118.84°, but in contrast with the very small change calculated in BN, 120.5°. This feature indicates that the C≡N substituent alone does not have any effect on its *ipso* angle.

(iii) The ring structure appears a little distorted. It shows a quinonoid structure, and thus with C1-C2 (C1-C6) and C3-C4 (C4-C5) bond lengths (1.40 Å at the MP2 level) longer than the C2-C3 (C5-C6) bonds, 1.39 Å. This effect is larger by DFT methods than by MP2. This quinonoid form is characteristic of BN molecule, with a C2-C3 bond length of 1.393 Å by MP2, and it remains in 4ABN with a value of 1.389 Å for this bond.

(iv) The ring angles at the C1 and C4 sites of substitution appear slightly closed, which leads to an opening of the angles at the vicinal C2 (C6) and very slightly at C3 (C5) atom positions.

(v) All the distortions can be explained in terms of the change in hybridization affected by the substituent at the carbon site to which it is appended. Thus, the ring angles obtained in 4A-2CBN can be reasonably explained by the superposition of the ring angular distortions of *ortho*-chlorobenzene, *para*-aminobenzene and BN, although the effect of the chlorine atom is small due to its low positive charge. It is as follows: starting from the symmetrical structure of benzene ring, the angle decreases slightly at the site of the -C≡N and -NH₂ substitutions and increases by ca 0.4–0.9° at adjacent positions. This is due to the electronegative C≡N substitution, which leads to a lengthening of the nearest C1-C2 bond and shortening of the vicinal C2-C3 (C6-C5) bonds, as observed in BN molecule, although with lower values.

(vi) The chlorine atom has no influence on the planarity of the structure. Thus, with the exception of the NH₂ group, 4A-2CBN is a planar molecule, as BN, i.e. all the ring torsional angles with values 0 or 180°.

(vii) The chlorine atom withdraws negative charge (0.22 *e*⁻ by MP2, where *e*⁻ is the charge of an electron) from the bonded C2 atom, which therefore changes to a small and positive value, Table 2. The effect of the NH₂ group is small on this atom, only there is a slight decrease in the negative charge, up to -0.126 *e*⁻.

The C–X and C≡N bonds

A notable difference in the computed C≡N and C4–N10 bond lengths is observed by the different methods used in the present study. At the MP2 level, the nitrile (C≡N) bond length is 1.184 Å, while by M06L it is 1.169 Å and by B3LYP/6-311++G(3df,pd) is 1.153 Å. For C4–N10 bond length, the differences are also large, with values 1.392 Å by MP2, 1.374 Å by M06L, and 1.377 Å by B3LYP6-311++G(3df,pd).

A small effect due to the chlorine atom on the C1–C7 bond length is observed (1.430 Å by MP2 in 4A-2CBN), which is slightly shorter as compared to BN (1.436 Å) and 4ABN (1.434 Å). The small reduction in 4ABN is mainly due to the –NH₂ group, which is a donor substituent on the ring. As the C≡N group remains almost unchanged, therefore, the substituents have no effect on the C≡N bond length.

Table 2. Calculated natural NBO atomic charges at B3LYP and MP2/6-31G(d,p) levels in 4A-2CBN and BN molecules.

Atom	4A-2CBN				BN	
	B3LYP/6-31-G(d,p)	B3LYP/6-311-++G(3df,pd)	M06L/6-31-G(d,p)	MP2/6-31-G(d,p)	B3LYP/6-31-G(d,p)	MP2/6-31-G(d,p)
C1	–0.224	–0.249	–0.223	–0.257	–0.171	–0.188
C2	0.012	0.021	0.013	0.051	–0.189	–0.17
C3	–0.302	–0.275	–0.306	–0.326	–0.235	–0.239
C4	0.203	0.202	0.213	0.275	–0.216	–0.198
C5	–0.291	–0.255	–0.293	–0.317	–0.235	–0.239
C6	–0.161	–0.114	–0.163	–0.113	–0.189	–0.17
C7	0.277	0.288	0.291	0.326	0.28	0.328
H8	0.256	0.22	0.252	0.254	0.247	0.243
N9	–0.827	–0.772	–0.835	–0.887	–	–
H10	0.245	0.21	0.241	0.243	0.247	0.243
H11	0.261	0.222	0.259	0.258	0.249	0.244
≡N	–0.305	–0.315	–0.322	–0.356	–0.305	–0.361
H13	0.414	0.383	0.42	0.412	–	–
H14	0.414	0.383	0.42	0.412	–	–
Cl	0.03	0.049	0.033	0.025	–	–

Although between 4A-2CBN and 4ABN, the differences in the C1–C7 and C–C bond lengths are small, however in the C4–N bond of the amino group, the difference is significant, and it is 1.392 Å in 4A-2CBN vs. 1.383 Å in 4ABN by MP2. This difference is due to the chlorine atom. The difference between 4ABN and aniline [72] is also significant. Thus, in 4ABN, the C4–N bond is shortened (1.383 Å vs 1.406 Å of aniline molecule), leading to a lower pyramidal character (more *sp*²) of the –NH₂ group, i.e. shortening of the N–H bond (1.010 Å in aniline molecule), opening of the C–N–H and H–N–H angles (113.0 and 109.8°, respectively in aniline), and lower inversion angle ω (34.7° in 4ABN vs 47.2° in aniline) and *tilt* angle ϵ (4.4° in aniline). This planarization of the amino group in 4ABN has been interpreted [68] due to resonance with the aromatic system.

4.2. Scaling the wavenumbers

The use of adequate quantum chemical methods and scaling procedures, compensates the calculated harmonic wavenumbers to be compared with the anharmonic wavenumbers found by the experiment (IR and Raman spectra) [73,74], and remarkably reduce the risk in the assignment of bands. The procedure selected for scaling the wavenumber depends on the size of the organic molecule and the accuracy required for the predicted wavenumber. In the present study following three scaling procedures were used:

(i) The linear scaling equation procedure (LSE), which employs the linear scaling equation calculated in the benzene molecule at the same level, that are the following:

$$v^{\text{scaled}} = 22.1 + 0.9543 \cdot \omega^{\text{calculated}} \quad \text{for B3LYP/6-31G(d,p) level, from [1,2]}$$

$$v^{\text{scaled}} = 23.6 + 0.9528 \cdot \omega^{\text{calculated}} \quad \text{for B3LYP/6-31G(d,p) level}$$

$$v^{\text{scaled}} = 31.2 + 0.9515 \cdot \omega^{\text{calculated}} \quad \text{for B3LYP/6-311++G(3df,pd) level}$$

$$v^{\text{scaled}} = 29.7 + 0.9502 \cdot \omega^{\text{calculated}} \quad \text{for M06L/6-31G(d,p) level}$$

The results are presented in Table 3. The calculated equation in the benzene molecule with the M06L method has a worse correlation coefficient r .

For the NH_2 vibrations, we used the following scaling equation which was obtained from the amino group of aniline molecule:

$$v^{\text{scaled}} = 44.5 + 0.9441 \cdot \omega^{\text{calculated}} \quad \text{for B3LYP/6-31G(d,p) level, from [72]}$$

$$v^{\text{scaled}} = 38.4 + 0.9367 \cdot \omega^{\text{calculated}} \quad \text{for M06L/6-31G(d,p) level}$$

Figures 2-5 show the experimental IR and Raman spectra, together with their simulated scaled spectra using the LSE procedure at the B3LYP/6-31G(d,p) level of theory.

(ii) The two linear scaling equations, one from 0-1000 cm^{-1} , and another one from 1000-4000 cm^{-1} . The equations used, presented for the first time here, were:

$$v^{\text{scaled}} = -21.0 + 1.0102 \cdot \omega^{\text{calculated}} \quad \text{for the 0-1000 } \text{cm}^{-1} \text{ range and B3LYP/6-31G(d,p)}$$

$$v^{\text{scaled}} = 32.5 + 0.9490 \cdot \omega^{\text{calculated}} \quad \text{for the 1000-4000 } \text{cm}^{-1} \text{ range and B3LYP/6-31G(d,p)}$$

$$v^{\text{scaled}} = -19.3 + 1.0157 \cdot \omega^{\text{calculated}} \quad \text{for the 0-1000 } \text{cm}^{-1} \text{ range and M06L/6-31G(d,p)}$$

$$v^{\text{scaled}} = 37.0 + 0.9469 \cdot \omega^{\text{calculated}} \quad \text{for the 1000-4000 } \text{cm}^{-1} \text{ range and M06L/6-31G(d,p)}$$

(iii) The polynomial scaling equation, $y = a + b_1x + b_2x^2$ where “y” is the scaled frequency, “x” is the calculated frequency, and “a”, “ b_1 ” and “ b_2 ” are coefficients determined in the benzene molecule. This scaling equation procedure is new and its accuracy has not been reported yet

$$v^{\text{scaled}} = -4.3 + 0.9923 \cdot \omega^{\text{calculated}} - 10.03 \cdot 10^{-6} \cdot (\omega^{\text{calculated}})^2 \quad \text{for B3LYP/6-31G(d,p) level}$$

$$v^{\text{scaled}} = 3.6 + 0.9871 \cdot \omega^{\text{calculated}} - 9.39 \cdot 10^{-6} \cdot (\omega^{\text{calculated}})^2 \quad \text{for M06L/6-31G(d,p) level}$$

4.3 Analysis of the different vibrations

In order to have the spectroscopic signatures of 4A-2CBN molecule, we performed calculations using B3LYP/6-31G(d,p), B3LYP/6-311++G(3df,pd), and M06-L/6-31G(d,p) methods. It is worthwhile to note that calculations were performed in gas phase, whereas spectra were recorded in solid samples, therefore there are some disagreements between calculated and observed vibrational wavenumbers. Table 3 collects the theoretical (calculated) results. The first column lists the computed wavenumbers at the B3LYP/6-31G(d,p) level in decreasing order, while the second column shows their respective relative IR intensities (A), and relative Raman scattering activities (S), third column. The relative IR and Raman intensities were determined by dividing the computed values by the intensity of the strongest ones at 1678 and 2345 cm^{-1} , respectively.

Table 3. Calculated harmonic wavenumbers (ω , cm^{-1}), relative infrared intensities (A, %), relative Raman scattering activities (S, %), Raman depolarization ratios for plane (P) and unpolarized (U) incident light, reduced mass (μ , amu), and force constant ($\text{mdyn}\cdot\text{\AA}^{-1}$, f) obtained in 4A-2CBN at different computational levels.

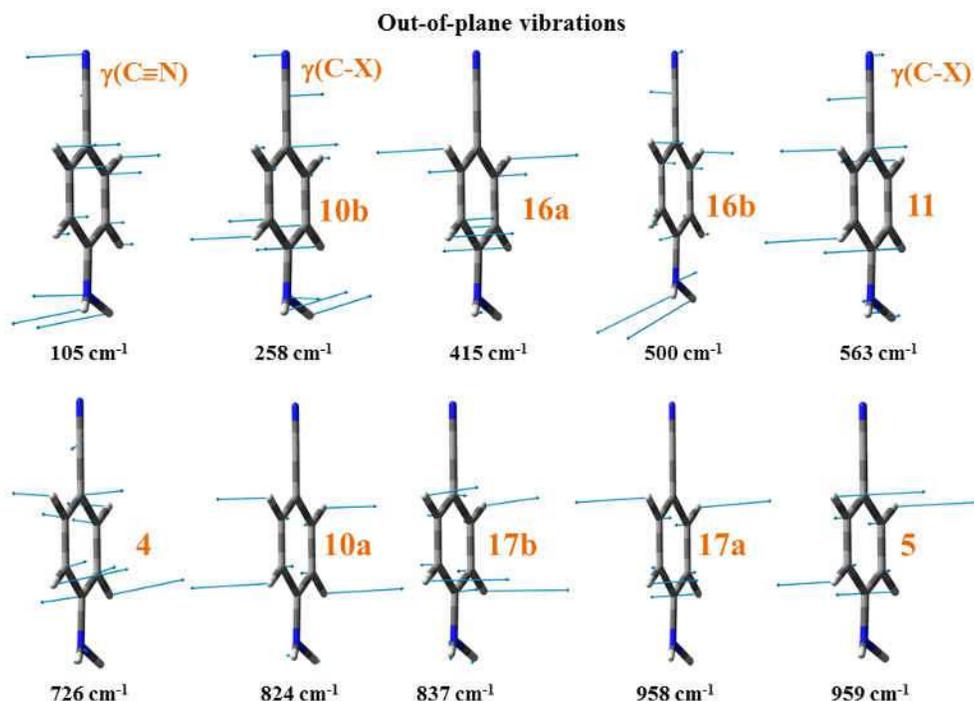
B3LYP/6-31G(d,p)				B3LYP/6-311++G(3df,pd)				M06L/6-31G(d,p)				Characterization
ω	A	S	ω	A	S	P	U	μ	f	ω	ω	
3217	1	28	3202	1	22	0.19	0.32	1.1	6.6	3228	3279	100%, 2, $\nu(\text{C-H})$ in C5-H, C6-H
3209	1	12	3194	1	9	0.27	0.42	1.1	6.6	3219	3268	100%, 20b, $\nu(\text{C-H})$ in C3-H
3192	2	17	3178	3	13	0.43	0.60	1.1	6.5	3211	3259	100%, 20a, $\nu(\text{C-H})$ in C5-H, C6-H
1657	15	11	1643	50	16	0.55	0.71	3.1	5.0	1669	1688	51%, 8a, $\nu(\text{C=C}) + 48\%$, $\beta_s(\text{NH}_2)$
1599	7	0	1585	9	0	0.36	0.53	6.0	8.9	1607	1639	98%, 8b, $\nu(\text{C=C})$
1541	22	5	1529	31	4	0.38	0.55	3.1	4.3	1550	1564	94%, 19b, $\nu(\text{C=C})$
1471	5	1	1461	6	1	0.41	0.58	3.0	3.8	1486	1502	97%, 19a, $\nu(\text{C=C})$
1355	2	2	1338	12	1	0.47	0.64	2.5	2.7	1389	1446	97%, 14, $\nu(\text{C=C})$
1351	16	1	1331	13	2	0.27	0.43	6.1	6.4	1364	1362	81%, 13, $\nu(\text{C-N, CCC}) + 18\%$, $\delta(\text{NH}_2)$
1280	10	4	1277	18	4	0.16	0.27	1.8	1.8	1280	1302	94%, 3, $\delta(\text{C-H})$
1241	0	7	1234	0	6	0.18	0.30	2.6	2.3	1247	1253	85%, 7a, $\nu(\text{C}\equiv\text{C, CCC}) + 13\%$, $\nu(\text{C}\equiv\text{N})$
1177	0	2	1175	1	1	0.18	0.30	1.3	1.0	1175	1195	100%, 18b, $\delta(\text{C-H})$
1060	12	0	1058	15	0	0.08	0.15	3.2	2.1	1070	1084	92%, 18a, $\delta(\text{C-H, CCC})$
958	0	0	972	0	0	0.72	0.83	1.3	0.7	951	942	99%, 5, $\gamma(\text{C-H})$ in C5-H, C6-H
924	8	4	922	10	5	0.06	0.11	5.3	2.7	936	882	70%, 1, $\delta(\text{CCC}) + 12\%$, $\delta(\text{NH}_2) + 10\%$, $\nu(\text{C-CL})$
852	8	0	872	8	0	0.31	0.48	1.6	0.7	847	806	95%, 17b, $\gamma(\text{C-H})$ in C3-H
826	7	1	830	9	0	0.60	0.75	1.5	0.6	813	780	95%, 11, $\gamma(\text{C-H})$ in C5-H, C6-H
724	1	0	724	0	0	0.31	0.47	3.9	1.2	730	730	55%, 12, $\delta(\text{CCC}) + 30\%$, $\delta(\text{C}\equiv\text{N}) + 13\%$, $\delta(\text{NH}_2)$
711	0	0	721	2	0	0.09	0.17	5.3	1.6	710	714	90%, 4, $\gamma(\text{CCC, C-C}\equiv)$
706	2	2	707	2	2	0.13	0.24	7.2	2.1	714	629	77%, 6b, $\delta(\text{CCC}) + 14\%$, $\nu(\text{C-CL})$
614	1	1	619	3	0	0.75	0.86	3.5	0.8	611	589	88%, 16b, $\gamma(\text{CCC}) + 10\%$, $\gamma(\text{C}\equiv\text{N})$
598	1	0	608	1	0	0.08	0.14	7.1	1.5	608	556	53%, 9b, $\delta(\text{C}\equiv\text{C, CCC}) + 32\%$, $\delta(\text{C}\equiv\text{N})$
462	38	3	461	15	3	0.18	0.30	3.9	0.5	461	459	40%, 6a?, $\delta(\text{C4-N, CCC}) + 37\%$, $\omega(\text{NH}_2) + 16\%$, $\delta(\text{C}\equiv\text{N})$
451	43	1	448	22	0	0.70	0.83	2.9	0.3	438	432	39%, 16a, $\gamma(\text{CCC}) + 38\%$, $\omega(\text{NH}_2) + 15\%$, $\gamma(\text{C}\equiv\text{N})$
401	0	0	403	0	0	0.26	0.42	4.1	0.4	404	398	48%, 15, $\delta(\text{C4-N, CCC}) + 27\%$, $\delta(\text{C}\equiv\text{N}) + 20\%$, $\delta(\text{NH}_2)$
389	2	1	391	2	1	0.60	0.75	13.5	1.2	395	390	45%, 7b, $\nu(\text{C-CL}) + 38\%$, $\delta(\text{C}\equiv\text{N}) + 17\%$, $\tau(\text{NH}_2)$
258	2	0	256	3	0	0.50	0.67	5.5	0.2	257	246	65%, 10b, $\gamma(\text{C4-N, CCC}) + 28\%$, $\gamma(\text{C}\equiv\text{N})$
245	0	0	246	0	0	0.70	0.83	6.3	0.2	245	245	60%, 9a, $\delta(\text{C-CL, ring}) + 21\%$, $\delta(\text{C}\equiv\text{N}) + 19\%$, $\tau(\text{NH}_2)$
182	0	0	181	0	0	0.75	0.86	5.2	0.1	176	178	74%, 10a, $\gamma(\text{C-CL, ring}) + 19\%$, $\gamma(\text{NH}_2)$
97	0	0	96	0	0	0.75	0.86	6.0	0.0	99	93	71%, $\tau(\text{structure}) + 16\%$, $\gamma(\text{C-C}\equiv) + 13\%$, $\gamma(\text{C-CL})$

The columns 4 to 10th collect the results at the B3LYP/6-311++G(3df,pd). In the column 7th is listed the Raman depolarization ratios for plane (P), and unpolarized incident light (U), 8th column, reduced masses (μ), 9th column, and the force constant of each vibration (f), 10th column. To check the accuracy of methods, the calculated wavenumbers at the M06L and MP2 levels are also listed in the columns 11-12th, respectively. In the last column appears the characterization established by B3LYP for each calculated wavenumber determined in the ring modes. For the characterization of the ring modes were taken into account the atomic displacement vectors obtained in 4ABN molecule, and plotted in Fig 6. For the assignment of the ring modes was followed the Varsanyi's notation [75] for a 1,2,4-tri-substituted benzene. The modes corresponding to the substituents appear listed in Table 4.

Table 4. Modes corresponding to the substituents in 4A-2CBN

Modes	4A-2CBN
Stretching	7a, 7b, 13
In-plane bending	9a, 9b, 15
Out-of-plane bending	10a, 10b, 17a

Table 5 collects the scaled values with the linear scaling equation procedure (LSE) at three levels of computation, together with the results obtained by the procedure that use two linear scaling equations and by the procedure that use a polynomial scaling equation. For simplicity, in the last both cases only two levels of computation were used. In the LSE procedure two linear equations were used at the B3LYP/6-31G(d,p) level: one with the scaling equation reported by us [1,2], and another one, with a new scaling equation calculated by us here with better values. In both cases the results were very similar. All the calculated scaled wavenumbers



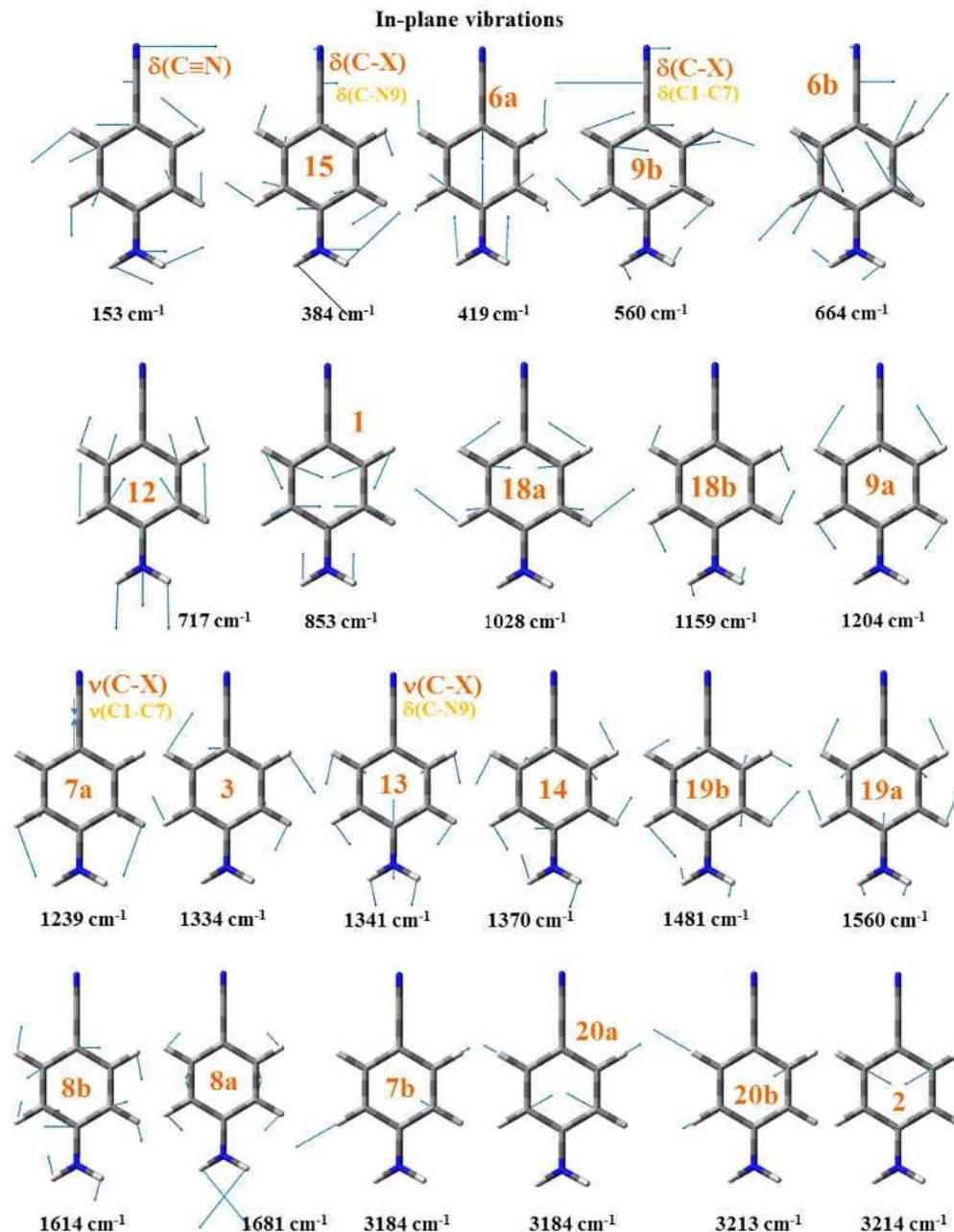


Fig 6. Characterization of the ring modes in 4-aminobenzonitrile molecule at the B3LYP/6-31G(d,p) level.

were compared to the experimental IR values obtained in KBr matrix and by Raman spectroscopy. Also for simplicity, the values obtained in Nujol mull were omitted in the Table because they appear very close to those in KBr matrix, Fig 4. The absolute error, $\Delta v = v(\text{scaled}) - v(\text{experimental})$ obtained for each method and procedure of scaling is included in the Table. The experimental values selected for this comparison appears underlined. Mainly they correspond to infrared values, and some cases, when it is observed an infrared value or it is not clear, from the Raman spectrum.

Table 5. Comparison of the scaled wavenumbers (ν , cm^{-1}) with different scaling procedures and at different DFT levels with the experimental values by IR and Raman spectroscopy, and the error obtained $\Delta\nu = \nu(\text{scaled}) - \nu(\text{experimental})$

B3LYP/6-31G (d,p) from [1,2]		scaling												Experimental		Assignment		
		LSE				Two eqns				polynomic				IR	Raman			
		B3LYP/6-31G (d,p)	B3LYP/6-311++ G(3df, pd)	M06L/6-31G (d,p)	M06L/6-31G (d,p)	B3LYP/6-31G (d,p)	M06L/6-31G (d,p)	B3LYP/6-31G (d,p)	M06L/6-31G (d,p)	B3LYP/6-31G (d,p)	M06L/6-31G (d,p)	B3LYP/6-31G (d,p)	M06L/6-31G (d,p)					
ν	$\Delta\nu$	ν	$\Delta\nu$	ν	$\Delta\nu$	ν	$\Delta\nu$	ν	$\Delta\nu$	ν	$\Delta\nu$	ν	$\Delta\nu$	ν	$\Delta\nu$	IR	Raman	Assignment
3092		3089		3078		3097		3085		3094		3084		3092		3127 vw	3127 vw	2, $\nu(\text{C-H})$ in C5-H, C6-H
3084	-8	3081	-11	3070	-22	3088	-4	3078	-14	3085	-7	3077	-15	3084	-8	3092 w	3085 vs	20b, $\nu(\text{C-H})$ in C3-H
3068	46	3065	43	3055	33	3081	59	3062	40	3077	55	3061	39	3076	54	3022 w	3030vw, 2925s	20a, $\nu(\text{C-H})$ in C5-H, C6-H
1603	21	1602	20	1595	13	1616	34	1605	23	1617	35	1612	30	1625	43	1582 s		8a, $\nu(\text{C=C}) + \beta_s(\text{NH}_2)$
1548	18	1547	17	1540	10	1557	27	1550	20	1559	29	1557	27	1566	36		1590 vs	8b, $\nu(\text{C=C})$
1493	-3	1492	-4	1486	-10	1503	7	1495	-1	1505	9	1501	5	1511	15	1496 vs	1530 w	19b, $\nu(\text{C=C})$
1426	-27	1425	-28	1422	-31	1442	-11	1428	-25	1444	-9	1434	-19	1450	-3	1453 vs	1455 m	19a, $\nu(\text{C=C})$
1315	-31	1315	-31	1305	-41	1350	4	1318	-28	1352	6	1322	-24	1357	11	1346 w	1386 m	14, $\nu(\text{C=C})$
1311	-3	1311	-3	1298	-16	1326	12	1315	1	1329	15	1318	4	1333	19	1314 s	1345 m	13, $\nu(\text{C4-N, CCC}) + \delta(\text{NH}_2)$
1244	-27	1243	-28	1247	-24	1246	-25	1247	-24	1249	-22	1249	-22	1252	-19	1271 vs	1320 w	3, $\delta(\text{C-H})$
1206	-1	1206	-1	1206	-1	1215	8	1210	3	1218	11	1212	5	1220	13	1207 sh	1279w, 1255w	7a, $\nu(\text{C-C}\equiv, \text{CCC}) + \nu(\text{C}\equiv\text{N})$
1145	-19	1145	-19	1150	-14	1146	-18	1149	-15	1150	-14	1150	-14	1150	-14	1164m, 1132w	1210s, 1191sh	18b, $\delta(\text{C-H})$
																1108m, 1132w	1178m, 1146w	18a, $\delta(\text{C-H, CCC})$
1034	-1	1034	-1	1038	3	1046	11	1038	3	1050	15	1036	1	1049	14	1008 m	1035m, 1015w	5, $\gamma(\text{C-H})$ in C5-H, C6-H
936	-14	936	-14	956	6	933	-17	947	-3	947	-3	937	-13	934	-16	950 m	975 w	1, $\delta(\text{CCC}) + \delta(\text{NH}_2) + \nu(\text{C-Cl})$
904	12	904	12	909	17	919	27	912	20	931	39	904	12	919	27	865vw, 892vw	871 w	17b, $\gamma(\text{C-H})$ in C3-H
835	-12	835	-12	861	14	835	-12	840	-7	841	-6	834	-13	833	-14	847 m	845 m	11, $\gamma(\text{C-H})$ in C5-H, C6-H
810	6	811	7	821	17	802	-2	813	9	806	2	808	4	800	-4	804 m	780 w	12, $\delta(\text{CCC}) + \delta(\text{C}\equiv\text{N}) + \delta(\text{NH}_2)$
713	-15	713	-15	721	-7	723	-5	710	-18	722	-6	709	-19	719	-9	728 vs	722 w	4, $\gamma(\text{CCC, C-C}\equiv)$
701	-9	701	-9	718	8	704	-6	697	-13	702	-8	696	-14	700	-10	710 sh		6b, $\delta(\text{CCC}) + \nu(\text{C-Cl})$
696	—	696	—	704	—	708	—	692	—	706	—	691	—	704	—			16b, $\gamma(\text{CCC}) + \gamma(\text{C}\equiv\text{N})$
608	-9	609	-8	621	4	610	-7	599	-18	601	-16	601	-16	603	-14		602 vs	9b, $\delta(\text{C-C}\equiv, \text{CCC}) + \delta(\text{C}\equiv\text{N})$
593	13	593	13	610	30	607	27	583	3	598	18	586	6	600	20	617 vw	582 vs	
																580 m		6a, $\delta(\text{C4-N, CCC}) + \omega(\text{NH}_2) + \delta(\text{C}\equiv\text{N})$
463	-3	464	-2	470	4	468	2	446	-20	449	-17	452	-14	457	-9		475 s	16a, $\gamma(\text{CCC}) + \omega(\text{NH}_2) + \gamma(\text{C}\equiv\text{N})$
452	41	453	42	458	47	446	35	435	24	426	15	441	30	434	23		411 m	15, $\delta(\text{C4-N, CCC}) + \delta(\text{C}\equiv\text{N}) + \delta(\text{NH}_2)$
405	—	406	—	415	—	414	—	384	—	391	—	392	—	401	—			7b, $\nu(\text{C-Cl}) + \delta(\text{C}\equiv\text{N}) + \tau(\text{NH}_2)$
393	10	394	11	404	21	405	22	372	-11	382	-1	380	-3	392	9		391 m	10b, $\gamma(\text{C4-N, CCC}) + \gamma(\text{C}\equiv\text{N})$
268	8	269	9	275	15	274	14	240	-20	242	-18	251	-9	257	-3	383 br,s	305m, 260m	9a, $\delta(\text{C-Cl, ring}) + \delta(\text{C}\equiv\text{N}) + \tau(\text{NH}_2)$
256	19	257	20	266	29	262	25	226	-11	230	-7	238	1	245	8	329 sh	237 m	10a, $\gamma(\text{C-Cl, ring}) + \gamma(\text{NH}_2)$
196		197		204		197		163		159		176		177		237 sh	220 m	$\tau(\text{structure}) + \gamma(\text{C-C}\equiv) + 13\% \gamma(\text{C-Cl})$
115	13	116	14	123	21	124	22	77	-25	81	-21	92	-10	101	-1	221sh, 216 sh	102 br, m	

vs: very strong, s: strong, m: medium, w: weak, vw: very weak, sh: shoulder, ν : stretching, br: broad, δ : in-plane bending, γ : out-of-plane bending, τ : torsion, ω : wagging, br: broad.

Table 6. The cyano and amino groups of 4A-2CBN. Comparison of the calculated harmonic wavenumbers (ω , cm^{-1}), relative infrared intensities (A, %), relative Raman scattering activities (S, %), Raman depolarization ratios for plane (P) and unpolarized (U) incident light, reduced mass (μ , amu), and force constant ($\text{mdyn}\cdot\text{\AA}^{-1}$, f) obtained at different levels. The scaled wavenumbers (ν , cm^{-1}) with the linear scaling equation are compared to the experimental values by IR and Raman spectroscopy.

		Calculated values										Scaled		Experimental		Assignment		
		B3LYP/6-31-G(d,p)					M06L/6-31G(d,p)					B3LYP/6-31G++G(3df,pd)	M06L/6-31G(d,p)	IR	Raman			
ω	A	S	ω	A	S	P	U	μ	f	ω	ν	ω	ν	ν	ν			
3710	7	16	3695	11	10	0.75	0.86	1.1	8.9	3752	3547	3758	3563	3553	3490 m	3510 s	100%, $\nu_{as}(\text{NH}_2)$	
3597	17	50	3591	24	43	0.16	0.27	1.0	7.9	3626	3448	3638	3455	3435	3420 w	3417 vs	100%, $\nu_s(\text{NH}_2)$	
1678	100	21	1661	100	10	0.48	0.65	1.4	2.3	1693	1612	1712	1623	1624	1640 m	1635 vs	61%, $\beta_s(\text{NH}_2)$ + 39%, δ_a , $\nu(\text{C}=\text{C})$	
1092	0	0	1085	0	0	0.58	0.73	1.4	1.0	1104	1064	1134	1064	1073	1052 m	1052 m	74%, $\tau(\text{NH}_2)$ + 24%, $\delta(\text{C-H})$	
436	37	0	431	89	1	0.51	0.68	1.5	0.2	438	442	406	438	449			51%, $\omega(\text{NH}_2)$ + 31%, $\gamma(\text{ring})$	
362	4	0	361	4	0	0.58	0.74	1.1	0.1	381	375	306	368	395	365 w	350 w	+12%, $\gamma(\text{C}\equiv\text{N})$	
																		85%, $\tau(\text{NH}_2)$ + 13%, $\gamma(\text{C-H})$
2345	17	100	2327	27	100	0.28	0.44	12.7	40.4	2323	2245	2204	2260	2210	2237 vs	2235 vs		
135	1	1	137	1	1	0.71	0.83	14.0	0.2	133	162	131	151	148	162 vs	162 vs	91%, $\nu(\text{C}\equiv\text{N})$	
515	4	1	519	4	0	0.75	0.86	8.7	1.4	519	526	478	514	511	558vw, 500m	560m, 520vw	50%, $\delta(\text{C}\equiv\text{N})$ + 25%, $\delta(\text{C-CL})$ + 17%, $\delta(\text{ring})$	
																		49%, $\gamma(\text{C}\equiv\text{N})$ + 37%, 17a, $\gamma(\text{C-C}\equiv\text{CCC})$

The values obtained in the substituent modes, C≡N and NH₂, are collected in Table 6. To understand the effect of substituents, these data were also compared with those obtained at the same computational level in 4ABN molecule. Only important modes are discussed in the present work. As the assignments for the remaining ring modes are obvious and therefore require no further discussion.

Table 7 collects the rms (the molecular root mean square error), the MAD (mean absolute deviation), the SD (the standard deviation), and the greatest positive and negative deviations from experiment for each level of computation and each procedure of scaling. It is worthwhile to note the following:

Table 7. The molecular-root-mean-square-error (rms), the mean-absolute-deviation (MAD), the standard deviation (SD), and the greatest positive and negative deviations from experiment for each level of computation and for the calculated and scaled wavenumbers of the ring modes of 4A-2CBN.

procedure	level	rms ^a	MAD	stan Dev	Large error	
					minimum	maximum
calculated	B3LYP/6-31G(d,p)	49.0	30.0	39.6	-5.0	170.0
	6-311++G(3df,pd)	43.7	27.8	34.3	-8.0	156.0
	M06L/6-31G(d,p)	55.7	34.7	44.4	-6.0	189.0
	MP2/6-31G(d,p)	73.6	48.3	56.5	-41.0	237.0
LSE	B3LYP/6-31G(d,p), from [1,2]	18.8	15.0	11.6	-31.0	46.0
	6-31G(d,p)	18.9	15.2	11.4	-31.4	42.9
	6-311++G(3df,pd)	21.2	17.6	11.9	-41.0	47.0
	M06L/6-31G(d,p)	21.3	16.9	13.2	-25.0	58.8
Two equations	B3LYP/6-31G(d,p)	18.0	15.3	9.8	-27.6	39.7
	M06L/6-31G(d,p)	19.9	15.6	12.5	-22.0	55.5
polynomic	B3LYP/6-31G(d,p)	17.2	14.2	9.9	-24.1	38.9
	M06L/6-31G(d,p)	20.1	16.0	12.4	-19.3	54.4

^arms, defined as $[\sum(\omega^{\text{cal.}} - v^{\text{exp.}})^2/n]^{1/2}$, where n is the number of wavenumbers considered. ^bMAD, defined as $[\sum|\Delta(\omega^{\text{cal.}} - v^{\text{exp.}})|]/n$

(i) MP2 calculated wavenumbers are the worst. Their values appear with very large overestimation and underestimation amounts, and its scaling (didn't included in the Table for simplicity) doesn't give the enough improvement to be considered.

(ii) The M06L scaled wavenumbers with the three scaling procedures appear in general with slightly lower accuracy than those by the B3LYP method.

(iii) With the B3LYP method the large basis set 6-311++G(3df,pd) does not represent an improvement on the scaled wavenumber, than that when it is used with the 6-31G(d,p) basis set.

(iv) Both LSE linear equations used at the B3LYP/6-31G(d,p) level lead to similar results.

(v) The best procedure of scaling is one which uses a polynomic equation, although the difference is small as compared to the other two procedures, by the LSE and by the two linear scaling equations.

Therefore, the discussion is mainly based on B3LYP/6-31G(d,p) results, and by those using the

polynomic scaling equation.

C-X (X = Cl, C≡, and N9) modes

The $\nu(\text{C-X})$ stretching vibrations corresponding to substituents are the normal modes **13**, **7a** and **7b**, [Table 4](#). Mode **13** corresponds to the amino substituent, $\nu(\text{C4-N})$, while **7b** is related to the chlorine atom, $\nu(\text{C-Cl})$, and mode **7a** to the cyano substituent, $\nu(\text{C-C}\equiv)$.

The in-plane bending, $\delta(\text{C-X})$ vibrations are the modes **15**, **9a** and **9b**. The mode **15** was identified corresponding to the amino substituent, $\delta(\text{C4-N})$, while mode **9a** to the chlorine atom, $\delta(\text{C-Cl})$, and mode **9b** to the cyano substituent, $\delta(\text{C-C}\equiv)$. The out-of-plane bending, $\gamma(\text{C-X})$ vibrations are the modes **17a**, **10a** and **10b**. According to the atomic displacement vectors, mode **10b** corresponds to $\gamma(\text{C4-N})$, while mode **10a** to $\gamma(\text{C-Cl})$ and **17a** to $\gamma(\text{C-C}\equiv)$.

C-Cl vibrations

The stretching vibrations belonging to the bond between the ring and the halogen atom generally give strong bands in the frequency range of 1130-480 cm^{-1} [76], and the wavenumber corresponding to these bands is influenced by the mass and bond strength of the neighboring substituents. Moreover, the smaller the halide atom the greater is the influence of the neighbor. In monochlorobenzene derivatives, such as in 4-chloro-3-nitrobenzonitrile [77], 2-amino-5-chlorobenzonitrile [78] and in 2-chloro-6-methyl benzonitrile [79], the C-Cl stretching wavenumber mainly appears in the 600-870 cm^{-1} range [75,80], whereas in dichlorobenzene derivatives, such as 2-amino-3,5-dichlorobenzonitrile [33], the main contributions are calculated at 397 and 381 cm^{-1} , and in 2,5-dichlorobenzonitrile they are computed at 459 and 330 cm^{-1} [56].

According to the Varsányi notation for a 1,2,4-trisubstituted benzene derivative, the $\nu(\text{C-X})$ stretching vibrations corresponding to the substituents are the normal modes **13**, **7a** and **7b**, [Table 4](#). In these modes that corresponding to the chlorine substituent is characterized as **7b**. The halogen atom directly attached to the benzene ring interacts with their vibrations. With a “heavy” substituent, as in our case, the stretching vibrations appear strongly coupled with CCC, NH_2 and $\text{C}\equiv\text{N}$ modes, and thus they are expected to be calculated below 600 cm^{-1} . Thus, in 4A-2CBN it was computed at 389 cm^{-1} (scaled at 380 cm^{-1} by polynomic scaling equation at the B3LYP level) and well related to the experimental IR and Raman bands at 383 and 391 cm^{-1} , respectively. Weak contributions of this C-Cl stretching mode were also determined in the calculated vibrations at 924 and 706 cm^{-1} .

$\delta(\text{C-Cl})$ in-plane bending vibration is better characterized as mode **9a**, and it appears strongly coupled with $\delta(\text{C}\equiv\text{N})$ bending and $r(\text{NH}_2)$ rocking modes. This C-Cl in-plane bending mode was related to the experimental IR and Raman bands at 237 cm^{-1} . Also, a high % PED of the C-Cl bending is calculated in the vibration at 135 cm^{-1} and characterized as $\delta(\text{C}\equiv\text{N})$.

In general, C-X out-of-plane vibrations are also coupled with the substituents vibrations, making difficult their identification. Mode **10a** appears coupled with $\gamma(\text{NH}_2)$ mode, and it was related to the $\gamma(\text{C-Cl})$ bending. By polynomic scaling equation it was scaled at 176 cm^{-1} , something far of the experimental IR and Raman bands at 216 and 220 cm^{-1} , respectively. Perhaps the anharmonic contribution of the $\gamma(\text{NH}_2)$ mode is responsible of this feature. A slight contribution of the $\gamma(\text{C-Cl})$ mode was also identified in the computed wavenumber at 97 cm^{-1} .

C1-C7≡ and C4-N9 vibrations

The C1-C7 \equiv stretching (mode **7a**) is identified in the calculated vibration at 1241 cm^{-1} (scaled at 1212 cm^{-1}), in accordance to that calculated in 4ABN at 1239 cm^{-1} [17]. It is predicted with almost null IR intensity and medium-strong Raman intensity, and it was correlated to the shoulder detected in the IR spectrum at 1207 cm^{-1} and to the strong Raman band at 1210 cm^{-1} . The atomic displacement vectors for this vibration look like mode **12**, instead of **7a**, according to the Varsányi description for a 1,2,4-trisubstituted

benzene derivative. Thus, for a better assignment of the modes in 4A-2CBN and to avoid possible mistakes, their atomic displacements vectors were compared to those of the ring modes in 4ABN and plotted Fig 6.

Similar feature appears in the C4-N9 stretching mode **13**, calculated at 1351 cm^{-1} (scaled at 1318 cm^{-1}) with strong IR intensity and weak-very weak Raman intensity, and good related to the experimental strong IR band observed at 1314 cm^{-1} and to the weak band at 1320 cm^{-1} in Raman. In 4ABN this mode is calculated at 1341 cm^{-1} . However, according to the atomic displacement vectors for this vibration in benzene molecule it should be better characterized as mode **1** instead of **13**. Figure 6 helps its assignment well as mode **13**.

The C-C \equiv in-plane bending (mode **9b**) was assigned to the computed wavenumber at 598 cm^{-1} , close to that calculated in 4ABN at 560 cm^{-1} . This mode is strongly coupled with the C \equiv N in-plane bending, with similar %PED as in 4ABN molecule. It appears scaled at 586 cm^{-1} in good accordance to the experimental IR band at 580 cm^{-1} and Raman line at 582 cm^{-1} .

Mode **15** corresponds to C4-N9 in-plane bending. Its characterization appears difficult due to the strong coupling with CCC, C \equiv N and NH₂ modes. It was calculated at 401 cm^{-1} , close to that at 384 cm^{-1} in 4ABN, i.e. the influence of the chlorine atom on this vibration is very less.

The highest %PED of the C-C \equiv out-of-plane bending mode **17a** appears in the computed wavenumber at 515 cm^{-1} , and mainly assigned as $\gamma(\text{C}\equiv\text{N})$ mode. In 4ABN the $\gamma(\text{C-C}\equiv)$ vibration corresponds to mode **11**, and it was calculated at 563 cm^{-1} [17].

Mode **10b** corresponds to the C4-N9 out-of-plane bending. It also appears strongly coupled with CCC and C \equiv N out-of-plane bending modes. It was calculated at 258 cm^{-1} , at exactly the same wavenumber as that in 4ABN, i.e. the chlorine atom has no influence on this C4-N9 out-of-plane mode.

Phenyl ring modes

C-H modes

These modes are little affected by the nature of substituents and usually appear above 3000 cm^{-1} as weak to moderate bands [81-82]. The calculated three stretching C-H vibrations (modes **2**, **20a** and **20b**) appear in a very close frequency range, with the frequency corresponding to C3-H bond in the middle of those between C5-H and C6-H bonds. The range predicted for these modes are in good accordance to our scaled and experimental wavenumbers, Table 5. The calculated IR intensity is in general weak-very weak, in agreement with that observed in the experimental spectrum, and with strong Raman intensity, also in accordance to that found experimentally.

The in-plane C-H bending vibrations of the phenyl ring are expected to appear in the range $1000\text{--}1300\text{ cm}^{-1}$ [81]. In the present study, the in-plane bending, $\delta(\text{C-H})$ mode **18b** is predicted at 1150 cm^{-1} , while mode **18a** is predicted at 1036 cm^{-1} with medium intensity, in good accordance to the experimental IR band at 1164 cm^{-1} (**18b**) and with the band of medium Raman intensity at 1035 cm^{-1} for **18a**. The IR band detected at 1008 cm^{-1} can be tentatively assigned to this mode. Mode **3** is computed with high IR intensity, scaled at 1249 cm^{-1} and well related to the very strong IR band at 1271 cm^{-1} .

The out-of-plane C-H bending vibrations of the phenyl ring are expected to appear in the range $700\text{--}1000\text{ cm}^{-1}$ [81]. In the present study, three out-of-plane bending, $\gamma(\text{C-H})$ modes: **17b**, **11** and **5** appear identified in the $780\text{--}975\text{ cm}^{-1}$ range, also in good accordance with our scaled values, Table 5. We cannot distinguish clearly the modes **11** and **17b** by their atomic displacement vectors. In benzene and 4ABN molecule, mode **17b** appears at a higher wavenumber than **11**. Thus, the same can also happen in 4A-2CBN molecule, and therefore we can tentatively assign the calculated wavenumber at 852 cm^{-1} as mode **17b** and that at 826 cm^{-1} as mode **11**. Modes **5** and **11** were related to the C5-H and C6-H bonds, while mode **17b** to C3-H bond. Modes **17b** and **11** are predicted with medium IR intensity, in accordance to that observed in the IR spectrum.

C=C modes

They are calculated strongly coupled with C-H modes and in several cases coupled with C≡N stretching and bending vibrations. The coupling with amino modes is very small. The tangential vibrations **8a**, **8b**, **19a**, **19b** and **14** belong to the stretching group. Modes **8** and **19** are in general fairly insensitive to substitution [67-70]. In 1,2,4-trisubstitution the frequency of the **8a** component is higher than that of **8b**, while the frequency of component **19b** is greater than that of **19a**. This feature can be explained by the potential energy contribution of the C-H in-plane bending vibrations associated to each mode, and when it is large the frequency of the vibration is high. Thus, this contribution is calculated greater in **8a** than in **8b**, with a reduced mass of 2.2 and 6.2 amu, respectively, at B3LYP/6-31G(d,p) level and therefore mode **8a** appears at higher wavenumber than **8b**.

Modes **19b** and **19a** were calculated at 1541 (**19b**) and 1471 (**19a**) cm^{-1} in 4A-2CBN vs 1525 cm^{-1} in benzene molecule [1-2]). According to Scherer in the Varsanyi book [75] this vibration couples very strongly with vibrational pair **18**, with similar motion of the hydrogen atoms. The strong IR intensity calculated for mode **19b** is in accordance to the very strong band observed experimentally. The assignment of mode **14**, the Kekule ring stretching mode, is usually difficult because the displacement vectors of the hydrogen atoms do not follow the directions as they appear in benzene molecule [1-2].

Radial skeletal vibrations correspond to modes **1**, **12**, **6a** and **6b**, and they appear coupled strongly with stretching and bendings C≡N modes. Mode **1** was calculated with medium-weak intensity at 924 cm^{-1} (scaled at 904 cm^{-1}) and was good related to the IR band observed in KBr matrix at 892 cm^{-1} . Also it is predicted with weak Raman intensity, in agreement to the weak Raman line at 871 cm^{-1} . Mode **12** appears strongly coupled with C≡N and NH₂ bending modes and it is calculated with weak IR intensity and almost null Raman intensity. It is scaled at 709 cm^{-1} (721 cm^{-1} at B3LYP/6-311++G(3df,pd) level) in accordance to the experimental IR band at 728 cm^{-1} and to the weak Raman band at 722 cm^{-1} . Mode **6b** was calculated at 706 cm^{-1} in agreement with that determined in 4ABN at 664 cm^{-1} [17].

The displacement vectors of the computed wavenumber at 462 cm^{-1} do not permit its clear identification. However, in 4ABN mode **6a** is calculated at 419 cm^{-1} [17], and accordingly we have assigned the calculated vibration at 462 cm^{-1} in 4A-2CBN to this mode. It is scaled at 452 cm^{-1} and, therefore, it was related to the IR band at 466 cm^{-1} and to the Raman band at 475 cm^{-1} .

Out-of-plane skeletal vibrations corresponding to modes **4**, **16a** and **16b** of benzene were also accurately determined. The frequency of the normal mode **4** is rather insensitive to substitution. Thus, it is calculated at 711 cm^{-1} vs. 718 cm^{-1} in benzene molecule and 726 cm^{-1} in 4ABN [17]. It is predicted with almost null IR and Raman intensity, scaled at 696 cm^{-1} and therefore it is related to the shoulder detected at 710 cm^{-1} . Modes **16a** appears strongly coupled with out-of-plane C≡N and NH₂ vibrations that cause a frequency increase. Thus, it was calculated at 451 cm^{-1} vs. 415 cm^{-1} in 4ABN and in benzene molecule. Mode **16b** is predicted with weak IR intensity and scaled at 601 cm^{-1} , and therefore it was excellently related to the very weak experimental IR band at 617 cm^{-1} and Raman line at 602 cm^{-1} .

Amino group modes

The calculated and scaled wavenumbers using the scaling procedure mentioned above for the different modes of the amino group are collected in Table 6, together with the experimental IR and Raman data and the assignment including the %PED.

The NH₂ group involves the symmetric (ν_{as}) and antisymmetric (ν_{sym}) N-H stretching vibrations. These modes can be easily identified and assigned on account of their characteristic magnitudes, however intramolecular bonding may lowers the magnitudes of these frequencies. The antisymmetric ν_{as} , stretching mode of NH₂ group appears calculated at a higher wavenumber (3710 cm^{-1} by B3LYP/6-31G(d,p)) than the symmetric ν_{s} one (3597 cm^{-1}). They were scaled by the LSE at 3563 and 3455 cm^{-1} , respectively, and they were related to the strong-very strong IR bands observed experimentally at 3510 and 3417 cm^{-1} , respectively.

The difference between theoretical and experimental can be attributed to intermolecular H-bonds in the solid state (not simulated in the present study) through this NH₂ group [72]. The predicted effect of the chlorine atom on these bands is very small. Thus, in 4ABN molecule they were computed at 3703 and 3591 cm⁻¹, respectively, only ca. 7 cm⁻¹ lower than to those calculated in 4A-2CBN. However, in the experimental IR bands the difference is larger, and in 4ABN [17] they were detected at 3490 (ν_{as}) and 3370 (ν_s) cm⁻¹ vs. 3510 (ν_{as}) and 3417 (ν_s) in 4A-2CBN. This large difference, which was not predicted theoretically, can be due to intermolecular H-bonds in the crystal through the NH₂ group which are stronger in 4ABN than in 4A-2CBN. Although there are no X-ray data of this molecule available in literature, the vibrational spectra in the solid state show that the chlorine atom in 4A-2CBN appears to reduce the strength of these H-bonds. As in other benzene derivatives [61], it is possible that in 4A-2CBN molecule the halogen atom forms intermolecular halogen bonds of type C-X...π (where X is a halogen atom). It is worthwhile to note that the calculated value of the intensity of ν_s mode is greater than ν_{as}, in agreement with that as observed in the IR spectra.

In the experimental IR spectrum of 4A-2CBN, two close strong bands were detected at 1635 and 1582 cm⁻¹ and on the basis of %PED they are assigned to the β_s(NH₂) and **8a** modes, respectively in consonance with two calculated strong bands which were scaled at 1623 and 1603 cm⁻¹. Both these modes appear to be coupled strongly and the % PED difference between them is: 61% of β_s(NH₂) in the band mainly assigned as β_s(NH₂), and 48% in the band assigned as mode **8a**. However, depending of the level of computation, this % PED can change and, therefore, the β_s(NH₂) mode can be assigned to a vibration at a wavenumber lower than that of mode **8a**, as it is predicted by M06L method, Tables 3 and 4. This feature is also observed in the case of 4ABN molecule [17].

Concerning the intensity, the scissoring mode β_s(NH₂) is calculated with the highest IR intensity, in accordance with that observed experimentally, which permits its clear identification in the spectra. The highest IR intensity computed for the β_s(NH₂) mode is also in accordance with that calculated in the aniline molecule [72]. However, in contrast, mode **8a** appears with intensity higher than β_s(NH₂) in the experimental Raman spectrum. This higher Raman intensity of mode **8a** than β_s(NH₂) was only accurately predicted by B3LYP/6-311++G(3df,pd).

The rocking mode of (NH₂) group, denoted as r (or δ_{as}), was scaled by B3LYP at 1064 cm⁻¹, almost at the same wavenumber obtained by M06L at 1062 cm⁻¹. In aniline molecule this mode appears strongly coupled with the **18a** ring mode [72]. However, in 4ABN and 4A-2CBN this coupling is weak, and r(NH₂) appears with a 74% PED. The chlorine atom slightly affects its wavenumber, thus it was scaled in 4ABN [17] at 1051 cm⁻¹ (calculated at 1078 cm⁻¹), and also with very weak or null IR and Raman intensity.

It seems extremely difficult to identify the experimental band corresponding to the position of the strongly anharmonic ω(NH₂) wagging vibration in the spectra of 4A-2CBN. In addition, this mode is sensitive to the intermolecular H-bonds through the NH₂ group. Therefore, we have not assigned this mode in the experimental spectra of 4A-2CBN, in agreement with previous authors [83]. However, on contrary in 4ABN the experimental band at 475 cm⁻¹ (IR) and 490 cm⁻¹ (Raman) have been assigned to this mode [17]. It is worthwhile to note that due to anharmonicity, mode mixing of inversion motion of hydrogen atoms of the NH₂ group with other out-of-plane motions cannot be described accurately, whereas in-plane normal mode motions can be reasonably modeled leading to lower errors .

The W(NH₂) mode in 4A-2CBN is calculated as the second strongest IR intensity band by B3LYP/6-311++G(3df,pd) and M06L/6-31G(d,p) with a relative IR intensity ca. 90, but by B3LYP/6-31G(d,p) it is lower with a relative IR intensity of 37, and in accordance with the experimental IR bands with weak-medium intensity which can be observed in the 400-500 cm⁻¹ range. This mode appears in the experimental spectra of aniline molecule and its derivatives as a very broad band with weak-medium intensity [72,84,85]. However, in the present case it was scaled by B3LYP/6-31G(d,p) at 438 cm⁻¹ using the linear scaling equation from the benzene molecule or at 456 cm⁻¹ using the equation from the amino group of aniline molecule [72]. The calculated wavenumber of W(NH₂) mode has little dependence on the basis set used, in accordance with

that observed in aniline molecule [72], but in contrast to that reported by other authors [19]. But, in aniline molecule, the value of wavenumber of this mode depends on the method used: by the B3LYP method and 6-31G(d,p) at 603 cm^{-1} , at 609.3 cm^{-1} with the 6-31+G(2d,p) basis, as well as with the 6-311++G(2d,p) at 608.0 cm^{-1} [71]. The computed wavenumber of this mode in 4A-2CBN, 436 cm^{-1} is lower than in aniline molecule [72] in accordance with a lower inversion angle ω calculated in 4A-2CBN molecule. At the B3LYP/6-311++G(3df,pd) level, the value in 4A-2CBN molecule is 31.5° (by X-ray is 34° [70]) while in aniline molecule [71] it is 39.7° .

Because the C_2 symmetry of the NH_2 group, the $\tau(\text{NH}_2)$ torsional band is not allowed by the IR selection rules. However, in the IR and Raman spectra can be identified a torsional band. This fact, as in the case of aniline molecule, was interpreted in Ref. [86,87] as combinations of the torsion and inversion vibrations (transit $1\leftarrow 0$), which are active in IR. In 4A-2CBN it is calculated at 362 cm^{-1} , which appears higher than calculated in 4ABN, 352 cm^{-1} , and in aniline molecule, 276 cm^{-1} . It can be explained as by the lowering of the inversion angle in 4A-2CBN and a shortening of the C-N bond, as compared to aniline molecule, which leads to an increment in the barrier height and hence to the wavenumber of the torsional mode. It is predicted with weak IR intensity at 368 cm^{-1} in accordance to the weak experimental IR band at 350 cm^{-1} . In 4ABN it has been assigned [17] to the experimental IR band at 330 cm^{-1} .

Vibrations of Nitrile ($\text{C}\equiv\text{N}$) group

The characteristic experimental wavenumber of $\text{C}\equiv\text{N}$ stretching vibrations of BNs falls ca. $2200\text{--}2300\text{ cm}^{-1}$ [80,88,89] with IR intensity which varies from medium-weak to strong depending on the substituents. However, as the geometry of the cyano group is not affected significantly by new substituents on the phenyl ring, therefore, their vibrational wavenumbers remain almost unchanged from the BN molecule [25,26]. In BN, $\nu(\text{C}\equiv\text{N})$ appears at 2230 cm^{-1} . Electron donating substituents, such as $-\text{NH}_2$, increase the IR intensity of $\nu(\text{C}\equiv\text{N})$ and decrease its frequency value, whereas the electron withdrawing groups ($-\text{F}$, $-\text{OH}$, and $-\text{Cl}$,) decrease the IR band intensity of $\nu(\text{C}\equiv\text{N})$ and increase its frequency to the higher limit of the characteristic spectral region [34,77,90-92].

In 4A-2CBN, the $\nu(\text{C}\equiv\text{N})$ stretching mode is highly localized on the $\text{C}\equiv\text{N}$ bond with a Potential Energy Distribution (PED) of 91%. It is slightly coupled with C1-C7 stretching to the extent of ca. 10%. It is calculated by all the methods with medium-strong IR intensity and very strong Raman intensity, the highest in the spectra. These results are in good agreement with the very strong experimental band observed at 2235 cm^{-1} in IR and at 2237 cm^{-1} in Raman spectra, and with the values obtained in other BNs [34]. The FTIR band intensity is slightly decreased by the electron withdrawing group ($-\text{Cl}$), while the Raman intensity is enhanced by the conjugation of the aromatic ring.

In the scaled bands at 713 , 696 , 593 cm^{-1} , and also in many bands below 500 cm^{-1} are determined contributions of the bending in-plane mode. However, the main contribution for the $\delta(\text{C}\equiv\text{N})$ mode is observed in the calculated band at 135 cm^{-1} with very weak IR intensity, and strongly coupled with C-Cl and ring bending vibrations. Due to this coupling, especially with the chlorine atom, this mode is calculated in 4A-2CBN at a lower wavenumber than in 4ABN molecule, 154 cm^{-1} .

The out-of-plane modes are identified in the calculated bands at 614 , 451 , 258 and 97 cm^{-1} , but the main contribution for the $\gamma(\text{C}\equiv\text{N})$ mode is observed in the calculated band at 515 cm^{-1} . This mode also appears strongly coupled with CC ring vibrations, and it is predicted with weak IR intensity and very weak Raman intensity in accordance with the experimental IR and Raman bands at 500 and 520 cm^{-1} , respectively.

Due to the linearity of the $\text{C}-\text{C}\equiv\text{N}$ bond, 179.9° by B3LYP/6-31G(d,p), sometimes the in-plane and out-of-plane bending vibrations appear calculated in reverse form, as in the present case with 4A-2CBN. Thus, $\delta(\text{C}\equiv\text{N})$ appears characterized at 135 cm^{-1} instead of at 515 cm^{-1} , $\gamma(\text{C}\equiv\text{N})$, and vice-versa. In other BN derivatives with other DFT methods, they are characterized in the right way. e.g. in 2,5-dichlorobenzonitrile [56] they are calculated at 621 cm^{-1} , $\delta(\text{C}\equiv\text{N})$ and at 138 cm^{-1} , $\gamma(\text{C}\equiv\text{N})$.

Combination bands

Several experimental Raman bands observed in the spectrum are far of the spectral range of the different ring modes and substituents modes. Thus, they can be assigned as combination bands: $1178+391=1569$ m, $871+391=1262$ m, and $780+475=1255$ w.

4.4 Other molecular properties

The values of the NBO atomic charges determined with the DFT and MP2 methods are listed in Table 2. For comparison purposes the calculated values in benzonitrile molecule are also included in the same Table. Some differences were observed between them. It is noted that the negative charge is mainly localized on the N9 atom, which produces the largest positive charge on the C4 atom. The chlorine atom has a very small positive charge. Thus, its effect on the BN structure is small, with a slight decrease in the positive charge on C7, and null effect on \equiv N atom.

The NBO atomic charges calculated by M06L method are in general larger than those calculated by B3LYP, but they are slightly lower than those calculated by MP2. The positive charge calculated by M06L on the chlorine atom is also larger than that calculated by B3LYP and MP2.

Thermodynamic parameters of 4A-2CBN were calculated and collected in Table 8. For an improvement in the determination of the Zero-Point Vibration Energies (ZPVE) and the entropy, $S_{\text{vib}}(T)$, the use of specific scale factors have been recommended [1-2], leading to the results shown in this Table. The translational, rotational and vibrational components are used to compute the entropy and free energy. The calculated values of the entropy by the three DFT methods appear very close and higher than those determined in BN molecule. These values of entropy indicate that as the temperature increases, the randomness of the molecules increases, i.e. the molecules will be distributed into a greater number of energy levels. At low temperatures, the translational energy levels contribute strongly to the behavior of entropy. Therefore, rotational and vibrational populations are distributed in a few low energy levels. At high temperatures, the vibrational population will be distributed in a larger number of vibrational levels, contributing to increase of entropy.

Table 8. Theoretical computed total energies and Gibbs Free energy (A.U.), rotational constants (GHz), entropies ($\text{cal}\cdot\text{mol}^{-1}\cdot\text{K}^{-1}$) and dipole moments (Debyes) at the B3LYP, M06L and MP2 levels in 4A-2CBN and BN molecules.

Parameters	4A-2CBN				BN	
	B3LYP/ 6-31G(d,p)	B3LYP/ 6-311++G (3df,pd)	M06L/ 6-31G(d,p)	MP2/ 6-31G(d,p)	B3LYP/ 6-31G(d,p)	MP2/ 6-31G(d,p)
Total energy + ZPE (AU)	0.346060 ^a	0.502477 ^a	0.288270 ^a	0.633023 ^b	0.400771 ^c	0.412258 ^d
Gibbs Free energy (AU)	0.380057 ^a	0.536457 ^a	0.322230 ^a	0.667270 ^b	0.431048 ^c	
Rotational constants (GHz)	1.87	1.89	1.9	1.89	5.65	5.65
	0.88	0.89	0.89	0.88	1.54	1.53
	0.6	0.61	0.61	0.6	1.21	1.21
Entropy ($\text{cal}\cdot\text{mol}^{-1}\cdot\text{K}^{-1}$)						
Total	92.02	91.96	91.84	93.12	78.56	79.44
Translational	40.97	40.97	40.97	40.97	39.8	39.81
Rotational	30.16	30.13	30.13	30.15	27.8	27.82
Vibrational	20.9	20.86	20.74	22.01	10.9	11.81
Dipole moments (Debyes)	7.55	7.51	7.74	7.37	4.55	5

^a -839. ^b -837. ^c -324. ^d -323.

A huge change is observed in the rotational constants. They were calculated very small as compared to BN. In the isolated state, by B3LYP they appear very close to those by MP2 and M06L methods.

The calculated dipole moment, Table 8, by M06L appears slightly higher than that calculated by MP2 and B3LYP, although the difference is small. The chlorine atom in 4A-2CBN has a little influence on the dipole moment of the molecule. Thus, the calculated value in 4-aminobenzonitrile is 6.53D by MP2 vs. 7.37 D in 4A-2CBN. The position in which the chlorine atom is bonded doesn't produce a remarkable change in the dipole moment, as compared to BN, but the effect of the NH_2 group is higher.

4.5MEP mapping

The other molecular properties like SCF energy, dipole moment, non-linear optical properties, HOMO-LUMO analysis and MEP mapping for the 4A-2CBN have been computed at B3LYP/6-311G(d,p) level of theory.

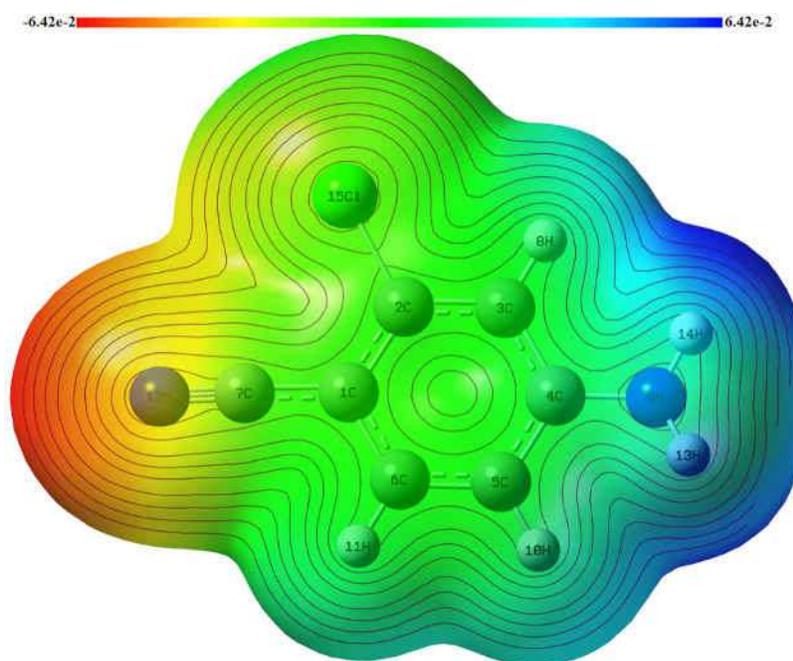


Fig 7. MEP diagram for the 4-amino-2-chlorobenzonitrile molecule

The molecular electrostatic potential (MEP) mapping has been used for understanding and predicting the sites of reactivity for electrophilic and nucleophilic reactions, investigation of biological recognition, hydrogen bonding interactions and other macroscopic properties [93]. The sign of the electrostatic potential in any particular site around a molecule that depends upon whether the effects of the nuclei or electrons are dominant is a key to assign its reactivity there [94]. The MEP surface is a plot of electrostatic potential mapped on to the constant electron density surface that represents the electrostatic potential in terms of colour coding [95,96], Fig 7. The surfaces with blue, green and red colours indicate the positive, zero and negative values of the potential, respectively. The red colour surfaces with negative MEP represent high electron density, whereas the blue colour surfaces with positive MEP correspond to areas of lowest electron density. MEP map for the 4A-2CBN is shown in Fig 7 with colour range from $-6.42e-2$ (deepest red) to $+6.42e-2$ (deepest blue). The surface over the hydrogen atom of NH_2 group shows maximum potential regions (dark blue).

coloured/ low electron density) as well as the relatively lower potential sites (light blue coloured) are around the other hydrogen atoms. The surface over the electronegative atom nitrogen (N7) represents the minimum potential (dark red coloured/ high electron density). The blue and red colour regions can be referred to as the site for nucleophilic and electrophilic attack, respectively. Thus, electrophiles (positively charged species) and nucleophiles (negatively charged species) will attack on the red and blue coloured sites, respectively. The regions over the ring and chlorine atom are neutral as characterized by green colour.

4.6 HOMO-LUMO analysis

The highest occupied molecular orbital (HOMO) and lowest unoccupied molecular orbital (LUMO) are main Molecular Orbitals that play important role in chemical reactions. The HOMO acts as an electron donor while LUMO acts as electron acceptor, and for 4A-2CBN molecule they are plotted in Fig 8. The energy gap between the HOMO and LUMO molecular orbitals helps to determine the chemical stability and electrical transport properties of molecules. The lowest excitation energy corresponds to HOMO-LUMO transition under TD-DFT approach which approximates the gap accurately. This gap was computed at TD-B3LYP/6-31G(d,p) level of theory. The low value of gap represents the high reactivity of the molecule in chemical reactions. The HOMO is delocalized over the all atoms and bonds C≡N, C1-C2, C1-C6, C3-C4, C4-C5, C3-H, C5-H, N-H13 and N-H14, except on H11 atom, while, the LUMO is delocalized over the bonds C2-C3, C1-C6, C5-C6, C6-H, C5-H, N-H13, N-H14 and over all atoms except H18. Thus, HOMO-LUMO excitation shows the charge transfer that can be seen in Fig 8. The low value of the energy gap explains the eventual charge transfer interactions taking place within the molecule. The SCF energy, dipole moment, HOMO, LUMO energy eigenvalues and energy gap computed at B3LYP/6-31G(d,p) level of theory are presented in Table 9.

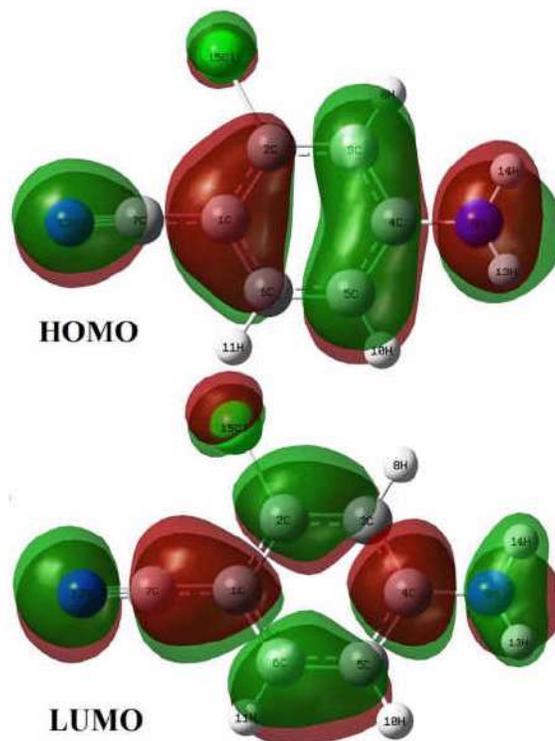


Fig 8. HOMO and LUMO plots for the 4-amino-2-chlorobenzonitrile.

Table 9. The SCF energy, HOMO, LUMO energy eigenvalues and HOMO-LUMO energy gap for the 4A-2CBN at the B3LYP/6-311G(d,p) level.

Energies	value
SCF energy (a.u.)	-839.452254
LUMO energy (eV)	-1.10
HOMO energy (eV)	-6.24
HOMO-LUMO gap (eV)	5.14
	4.68 ^a

^a approximated by using TD-B3LYP/6-31G(d,p) calculation

4.7 NLO properties

DFT calculations play an important role in designing the non-linear optical molecules. The molecules having the larger hyperpolarizability value show a strong NLO potential and can be used in fabrication of many optical devices. The molecules having donor-acceptor group attached to an aromatic ring increases the charge transfer through p-electron delocalization and give rise the hyperpolarizability values [97]. The polarizability, first order hyperpolarizability values and mean first order hyperpolarizability of the 4A-2CBN molecule were computed at B3LYP/6-31G(d,p) level of theory and they are presented in Table 10. The mean first hyperpolarizability of 4A-2CBN is 4.127×10^{-30} esu, which is 11 times greater than that of urea (for urea β_0 is 0.3728×10^{-30} esu) [93]. Thus, the high value of dipole moment and first order hyperpolarizability are representing the NLO potential of 4A-2CBN molecule.

Table 10. Calculated components of polarizability (a.u.), first order hyperpolarizability (a.u.), mean polarizability $\langle \alpha \rangle$ (a.u.), anisotropy of the polarizability γ (a.u.) and the mean first order hyperpolarizability β_0 (esu, 1 a.u. = 8.639×10^{-33} esu) of 4A-2CBN.

	B3LYP/6-31G(d,p)		B3LYP/-31G(d,p)
α_{xx}	149.02	β_{xxx}	-458.69
α_{xy}	7.56	β_{xxy}	-283.47
α_{yy}	101.29	β_{xyy}	73.63
α_{xz}	-1.80	β_{yyy}	-3.90
α_{yz}	-0.44	β_{xxz}	42.70
α_{zz}	34.65	β_{xyz}	11.82
$\langle \alpha \rangle$	94.99	β_{yyz}	6.46
γ	100.40	β_{xzz}	4.61
		β_{yzz}	2.72
		β_{zzz}	0.50
		β_0 (esu) $\cdot 10^{-30}$	4.13

5 Summary and Conclusions

In this paper, we attempted to provide a more comprehensive structural and vibrational study of 4A-2CBN by combining both theoretical and experimental data for the first time. Quantum chemical calculations were done to support the experimental results. Two conformations were computed in 4A-2CBN, with the $-\text{NH}_2$ group in planar form being a saddle point. The most important findings of the present work are the following:

(1) From the point of view of accuracy of the method, the equilibrium geometry calculated by the new M06L method in 4A-2CBN was compared with those obtained by B3LYP and MP2. In the calculated C-C bond lengths, M06L appears with the same accuracy as that by B3LYP, however at least by B3LYP with the 6-31G(d,p) basis set used, the C≡N and C-Cl bond lengths are computed worse.

(2) To improve the accuracy in the assignment of the calculated wavenumbers in the 4A-2CBN molecule, three different scaling equations procedures have been used. The best procedure of scaling is which uses a polynomial equation, although the difference is small as compared to the other two procedures, by the LSE and by the two linear scaling equations. Low errors were in general obtained in the scaled values.

(3) For the first time the polynomial scaling equation, $y = a + b_1x + b_2 x^2$ procedure has been presented and used in the 4A-2CBN molecule. Its accuracy has been determined.

(4) The M06L scaled wavenumbers appear in general with slightly lower accuracy than by B3LYP method

(5) The calculated linear scaling equation by M06L with the benzene molecule leads to worse correlation coefficient r than by B3LYP. However, the relative IR and Raman intensities predicted by the three DFT methods are very similar. In general, the bands calculated by M06L appear shifted to higher wavenumbers related to those calculated by B3LYP and with larger errors as compared to the experimental results. Thus worse scaled wavenumbers are obtained with the M06L method, and therefore it is not recommended for its use, at least with the 6-31G(d,p) basis set. Further calculations with other molecules and basis set are required to confirm this feature.

(6) The IR spectra of 4A-2CBN, in KBr matrix and in Nujol and as well its Raman spectrum in the solid state, were recorded and the bands observed were assigned accurately for the first time.

(7) The assignments of the observed IR and Raman bands find support from related molecules and are consistent with the established ranges of the vibrations of the different modes. Therefore, they seem to be the most accurate today.

(8) The main effect of the chlorine atom on the BN structure is a slight shortening of the C4-N and Cl-C≡ bond lengths. Also it withdraws negative charge on the bonded atom C2. As a consequence, a small shortening of C2-C3 and C5-C6 bond lengths is observed as compared to BN, and a lengthening of C1-C2, and angles slightly out of the regular hexagonal structure.

(9) As compared to MP2, the NBO atomic charges calculated by M06L are in general slightly better than those obtained by B3LYP. DFT methods appear to fail in the calculated charges on C4, C6 and N9 atoms.

(10) The quinonoid structure of the BN molecule remains in 4A-2CBN, although its symmetry appears slightly modified by the chlorine atom.

(11) In general C=C modes appear strongly coupled with C-H and C≡N modes, while the amino modes appear as almost pure modes with very small coupling with other modes.

(12) The size, shape, charge density distribution and structure activity relationship of the 4A-2CBN molecule were obtained by mapping electrostatic potential surface on the electron density isosurface. HOMO-LUMO energy was also computed. The high value of dipole moment and first order hyperpolarizability represent the NLO potential of 4A-2CBN molecule.

Acknowledgement

MAP wishes to thank NILS Science and Sustainability Programme (ES07), 002-ABEL-CM-2014A Call for financial support. Supported by a grant from Iceland, Liechtenstein and Norway through the EEA

Financial Mechanism. Operated by Universidad Complutense de Madrid. The authors (DB, and VKR) are thankful to Sri Rakesh Mohan Garg, Chairman R D Group of Institutions, Kadrabad, Ghaziabad, India, for providing computer facility in the Institute.

References

1. Palafox M A, Recent Research Developments in Physical Chemistry, India: Transworld Research Network, 2 (1998) 213-232.
2. Palafox M A, *Int J Quantum Chem*, 77(2000)661-684.
3. Palafox M A, Rastogi V K, *Spectrochim Acta*, A 58(2002)411-440.
4. Palafox M A, Rastogi V K, Mittal L, *Int J Quantum Chem*, 94(2003)189-204.
5. Palafox M A, Rastogi V K, Mittal L, Kiefer W, Mital H P, *Int J Quantum Chem*, 106(2006)1885-1901.
6. Imahori H, El Khouly M E, Fujitsuka M, Ito O, Sakata Y, Fukuzumi S, *J Phys Chem B*, 101(2001)325-332.
7. (a) Butera J A, Antane M M, Antane S A, Argentieri T M, Freedden C, Graceffa R F, Hirth B H, Jenkins D, Lennox J R, Matelan E, Norton N W, Qluagliato D, Sheldon J H, Spinelli W, Warga D, Wojdan A, Woods M, *J Med Chem*, 43(2000)1187-1202.
(b) Butera J A, Antane M M, Antane S A, Argentieri T M, Freedden C, Graceffa R F, Hirth B H, Jenkins D, Lennox J R, Matelan E, Norton N W, Qluagliato D, Sheldon J H, Spinelli W, Warga D, Wojdan A, Woods M, *J Med Chem*, 43(2000)1203-1214.
8. Kagara K, Goto S, Ichihara M, *J Synt Org Chem Jpn*, 57(1999)415-421.
9. Fadda A A, Afash M El-Sayed, Awad R S, *Eur J Med Chem*, 60(2013)421-430.
10. Zhang S, Zhang Y, Ma X, Lu L, He Y, Deng Y J, *J Phys Chem B*, 117(2013)2764-2772.
11. Tan W, Zheng D, Wu H, Zhu D, *Tetrahedron Lett*, 49(2008)1361-1364.
12. Peng L, Zhang L, Cheng X, Feng L S, Hao H Q, *Plant Biol*, 15(2013)404-414.
13. Veselá A B, Pelantová H, Sülc M, Macková M, Lovecká P, Thimová M, Pasquarelli F, Pičmanová M, Pátek M, Bhalla T C, Martinkova L, *J Ind Microb Biotechnol*, 39 (2012)1811-1819.
14. Koopman H, Daams J, *Weed Research*, 5(1965)319-326.
15. Björklund E, Styrihave B, Anskjær G G, Hansen M, Sørensen B H, *Sci Total Environ*, 409(2011)3732-3739.
16. Agarwal P, Bee S, Gupta A, Tandon P, Rastogi V K, Mishra S, Rawat P, *Spectrochim Acta*, A 121(2014)464-482.
17. Palafox M A, Rastogi V K, Vats J K, *J Raman Spectrosc*, 37(2006)85-99.
18. Vujovic D, Raubenheimer H G, Nassimbeni L R, *Eur J Inorg Chem*, 14(2004)2943-2949.
19. Kolek P, Pirowska K, Najbar J, *Phys Chem Chem Phys*, 3(2001)4874-4888.
20. Kolek P, Pirowska K, Chacaga L, Najbar J, *Phys Chem Chem Phys*, 5 (2003)4096-4107.
21. Kolek P, Pirowska K, Gora M, Kozik B, Najbar J, *Chem Phys*, 285(2002)55-72.
22. Rastogi V K, Jain D K, Sharma Y C, *Asian J Chem*, 3(1991)113-115.
23. Rastogi V K, Palafox M Alcolea, Lal B, Jain V, *Indian J Pure Appl Phys*, 38(2000)564-569.
24. Singh N P, Yadav R A, *Indian J Phys*, B75(2001)347-355.
25. Rastogi V K, Palafox M Alcolea, Singhal S, Ojha S P, Kiefer W, *Int J Quantum Chem*, 107(2007)1099-1114.
26. Rastogi V K, Singhal S, Kumar A P, Rao G R, Palafox M Alcolea, *Indian J Pure Appl Phys*, 47(2009)844-851.
27. Palafox M Alcolea, Rastogi V K, In Perspectives in Modern Optics & Optical Instrumentation, Joseph J, Sharma A, Rastogi V K, Eds; Anita Publications, FF-43, Managal Bazar, Laxminagar, Delhi, Ghaziabad, India, 2002, 91-98.
28. Sudha S, Sundaraganesan N, Kurt M, Cinar M, Karabacak M, *J Molec Struct*, 985(2011)148-156.
29. Nataraj A, Balachandran V, Karthick T, *J Molec Struct*, 1038(2013)134-144.
30. Jeyavijayan S, Arivazhagan M, *Spectrochim Acta*, A 81(2011)466-474.

31. Rastogi V K, Arora C B, Singhal S K, Singh D N, Yadav R A, *Spectrochim Acta*, A 53(1997)2505-2510.
32. Rastogi V K, Jain V, Palafox M Alcolea, Singh D N, Yadav R A, *Spectrochim Acta*, A 57(2001)209-216.
33. Rastogi V K, Palafox M Alcolea, Tomar R, Singh U, *Spectrochim Acta*, A 110(2013)458-470.
34. Rastogi V K, Palafox M Alcolea, Tanwar R P, Mittal L, *Spectrochim Acta*, A 58(2002)1987-2004.
35. Sundaraganesan N, Meganathan C, Joshua B D, Mani P, Jayaprakash A, *Spectrochim Acta*, A 71(2008)1134-1139.
36. Krishnakumar V, S Dheivamalar, *Spectrochimica Acta*, A 71(2008)465-470.
37. Goyal Y, Alam M Jane, Bhat D, Ahmad S, Palafox M Alcolea, Rastogi V K, Fifth International Conference on Perspectives in vibrational spectroscopy (ICOPVS-2014), Kerala (India) (2014).
38. Rasheed Tabish, Ahmad Shabbir, *Spectrochim Acta*, A 77(2010)446-456.
39. Seminario J M, Politzer P (Eds), *Modern density functional theory: a tool for chemistry*, Vol 2, (Elsevier Amsterdam), 1995.
40. Palafox M A, Tardajos G, Kim J J, Nielsen O F, Lodhi R, Rastogi V K, *Asian J Phys*, 15(2006)281-285.
41. Ponomareva A G, Yurenko Y P, Zhurakivsky R O, van Mourik T, Hovorun D M, *Phys Chem Chem Phys*, 14(2012) 6787-6795.
42. Shishkin O V, Pelmenchikov A, Hovorun D M, Leszczynski J, *J Molec Struct*, 526(2000)329-341.
43. Shishkin O V, Gorg L, Zhikol O A, Leszczynski J, *J Biomol Struct Dyn*, 21(2004)537-553.
44. Shishkin O V, Gorg L, Zhikol O A, Leszczynski J, *J Biomol Struct Dyn*, 22(2004)227-243.
45. Palamarchuk G V, Shishkin O, Gorb V L, Leszczynski J, *J Biomol Struct Dyn*, 26(2009)653-661.
46. Brovarets O O, Hovorun D M, *J Biomol Struct Dyn*, 32(2014)127-154.
47. Palafox M Alcolea, *J Biomol Struct Dyn*, 32(2014)831-851.
48. (a) Palafox M Alcolea, Posada-Moreno P, Villarino-Marín A L, Martínez-Rincon C, Ortuño-Soriano I, Zaragoza-García I, *J Comput Aided Molec Design*, 25(2011)145-161.
(b) Alvarez-Ros M C, Palafox M Alcolea, *Pharmaceuticals*, 7(2014)695-722.
49. Hoffmann M, Rychlewski J, *Rev Mod Quant Chem*, 2(2002)767.
50. Arjunan V, Raj A, Anitha R, Mohan S, *Spectrochim Acta*, A 125(2014)160-174.
51. Arjunan V, Govindaraja S T, Jose S P, Mohan S, *Spectrochim Acta*, A 128(2014)22-36.
52. Arjunan V, Devi L, Subbalakshmi R, Rani T, Mohan S, *Spectrochim Acta*, A 130(2014)164-177.
53. Sundaraganesan N, Mariappan G, Manoharan S, *Spectrochim Acta*, A 87(2012)67-76.
54. Szafran M, Ostrowska K, Katrusiak A, Dega-Szafran Z, *Spectrochim Acta*, A 128(2014)844-851.
55. Kattan D, Palafox M Alcolea, Kumar S, Manimaran D, Joe H, Rastogi V K, *Spectrochim Acta*, A 123(2014)89-97.
56. Palafox M A, Bhat D, Goyal Y, Ahmad S, Joe I Hubert, Rastogi V K, *Spectrochim Acta*, A136(2015)464-472.
57. Palafox M A, Jothy V B, Singhal S, Joe I Hubert, Kumar S, Rastogi V K, *Spectrochim Acta*, A 116(2013)509-517.
58. Zhao Y, Truhlar D G, *J Chem Phys*, 125(2006)194101; doi.org/10.1063/1.2370993
59. Gaussian 09, Revision D.01, Frisch M J, Trucks G W, Schlegel H B, Scuseria G E, Robb M A, J.R. Cheeseman J R, Scalmani G, Barone V, Mennucci B, Petersson G A, Nakatsuji H, Caricato M, Li X, Hratchian H P, Izmaylov A F, Bloino J, Zheng G, Sonnenberg J L, Hada M, Ehara M, Toyota K, Fukuda R, Hasegawa J, Ishida M, Nakajima T, Honda Y, Kitao O, Nakai H, Vreven T, Montgomery J A (Jr), Peralta J E, Ogliaro F, Bearpark M, Heyd J J, Brothers E, Kudin K N, Staroverov V N, Kobayashi R, Normand J, Raghavachari K, Rendell A, Burant J C, Iyengar S S, Tomasi J, Cossi M, Rega N, J.M. Millam, M. Klene, J.E. Knox, J.B. Cross, V. Bakken, C. Adamo, Jaramillo J, Gomperts R, Stratmann R E, Yazyev O, Austin A J, Cammi R, Pomelli C, Ochterski J W, Martin R L, Morokuma K, Zakrzewski V G, Voth G A, Salvador P, Dannenberg J J, Dapprich S, Daniels A D, Farkas Ö, Foresman J B, Ortiz J V, Cioslowski J, Fox D J, Gaussian, Inc., Wallingford CT, 2009.
60. Zhao Y, Truhlar D G, *Chem Phys Lett*, 502(2011)1-13.

61. Sert Y, Mirosław B, Çırak C, Doğan H, Szulczyk D, Struga M, *Spectrochim Acta*, A 128(2014)91-99.
62. Carpenter J E, Weinhold F, *J Molec Struct* (Theochem), 169(1988)41-62.
63. Reed A E, Curtiss L A, Weinhold F, *Chem Rev*, 88(1988)899-926.
64. Polavarapu P L, *J Phys Chem*, 94(1990)8106-812.
65. Kerestztury G, Holy S, Varga J, Bensenya G, Wang A Y, Rurig J R , *Spectrochim Acta*, A49(1993)2007-2026.
66. Kerestztury G, Raman spectroscopy theory, in J M Chalmers. P R Griffiths (Eds). *Handbook of Vibrational Spectroscopy*, vol 1, (Wiley), 2002, pp 71-87.
67. Casado J, Nygaard L, Sørensen G O, *J Molec Struct*, 8(1971)211-224.
68. Islor A M, Chandrakantha B, Gerber T, Hosten E, Betz R, *Z Kristallogr NCS*, 228(2013)217-218; doi: 10.1524/nrcs.2013.0107.
69. Merlino S, Sartori F, *Acta Crystallogr*, B38(1982)1476-1480.
70. Heine A, Herbst-Irmer R, Stalke D, *Acta Crystallogr*, B50(1994)363-373.
71. Palafox M Alcolea, Núñez J L, Gil M, *J Molec Struct*. (Theochem), 593(2002)101-131.
72. Palafox M Alcolea, Gil M, Núñez J L, Rastogi V K, Mittal L, Sharma R, *Int J Quantum Chem*, 103(2005)394-421.
73. Palafox M Alcolea, Rastogi V K, *Spectrochim Acta*, A 58(2002)411-440.
74. Palafox M Alcolea, Núñez J L, Gil M, Rastogi V K, *Perspectives in Engineering Optics*, Singh K, Rastogi V K, Eds, Anita Publications, Delhi-Ghaziabad, (2002), 356-391.
75. Varsanyi G, *Assignments for vibrational Spectra of Seven hundred benzene derivatives*, Vol 1, Adam Hilger, London, 1974, pp. 280.
76. (a) Mooney E F, *Spectrochim Acta*, 20(1964)1021-1032.
(b) Mooney E F, *Spectrochim Acta*, 19(1963)877-887.
77. Sert Y, Çırak C, Ucun F, *Spectrochim Acta*, A 107(2013)48-255.
78. Lakshmaiah B, Rao G R, *J Raman Spectrosc*, 20(1989)439-448.
79. Kumar V, Panikar Y, Palafox M Alcolea, Vats J K, Kostova I, Lang K, Rastogi V K, *Indian J Pure & Appl Phys*, 48(2010)85-94.
80. Faniran J A, Iweibo I, Oderinde R A, *J Raman Spectrosc*, 11(1981)477-480.
81. Roeges N P, *A Guide to the complete interpretation of infrared spectra of organic structures*, (Wiley, New York), 1994.
82. Coates J, *Encyclopedia of Analytical Chemistry*, in. R.A. Meyers (ed) *Interpretation of Infrared Spectrum: A Practical Approach*, (John Wiley, Chichester), 2000.
83. Ram S, Yadav J S, Rai D K, *Ind J Phy*, 59B(1985)19-28.
84. Palafox M Alcolea, *Asian J Phys*. 2(1993)72-80.
85. Palafox M Alcolea, *Ind J Pure Appl Phys*, 30(1992)59.
86. Palafox M Alcolea, *J Molec Struct*, 175(1988)81-84.
87. Larsen N W, Hansen E L, Nicolaisen F M, *Chem Phys Lett*, 43(1976)584-586.
88. Lin-Vien D, Colthup N B, Fateley W G, Grasselli J G, *The Handbook of Infrared and Raman Characteristic frequencies of Organic Molecules*, (Academic Press Inc, San Diego, California), 1991.
89. Dollish F R, Fateley W G, Bentley F F, *Characteristic Raman Frequencies of Organic Compounds*, (Wiley, New York 1974).
90. Arivazhagan M, Meenakshi R, Prabhakaran S, *Spectrochim Acta*, A 102(2013)59-65.
91. Arjunan V, Carthigayan K, Periandy S, Balamurugan K, Mohan S, *Spectrochim Acta*, A 98(2012)156-169.
92. Dheivamalar S, Silambarasan V, *Spectrochim Acta*, A 96(2012)480-484.
93. Arivazhagan M, Kumar J S, *Indian J Pure Appl Phys*, 50(2012)363-373.
94. Sapse A M, *Molecular Orbital Calculations for Biological Systems*, (Oxford University Press, New York), 1998.

95. Alam M J, Ahmad S, *Spectrochim Acta*, A 128(2014)653-664 and ref. cited therein.
96. Alam M J, Ahmad S, *J Molec Struct*, 1059(2014)239-254.
97. <http://www.sigmaaldrich.com/materials-science/organic-electronics/photonic-optical-materials/tutorial/nlo-materials.html>

[Received: 25.1.2016; revised recd: 12.2.2016; accepted: 28.2.2016]